(4)

David Taylor Research Center
Bethesda, MD 20084–5000

DTRC–SME–89/76 September 1990
Ship Materials Engineering Department
Research & Development Report

Electrochemical Impedance of Organic Coated Steel; Final Report—Correlation of Impedance Parameters with Long–Term Coating Performance

by
John N. Murray
Harvey P. Hack

DTRC–SME–89/76 Electrochemical Impedance of Organic Coated Steel; Final Report—
Correlation of Impedance Parameters with Long–Term Coating Performance

MAJOR DTRC TECHNICAL COMPONENTS

CODE 011 DIRECTOR OF TECHNOLOGY, PLANS AND ASSESSMENT

12 SHIP SYSTEMS INTEGRATION DEPARTMENT

14 SHIP ELECTROMAGNETIC SIGNATURES DEPARTMENT

15 SHIP HYDROMECHANICS DEPARTMENT

16 AVIATION DEPARTMENT

17 SHIP STRUCTURES AND PROTECTION DEPARTMENT

18 COMPUTATION, MATHEMATICS & LOGISTICS DEPARTMENT

19 SHIP ACOUSTICS DEPARTMENT

27 PROPULSION AND AUXILIARY SYSTEMS DEPARTMENT

28 SHIP MATERIALS ENGINEERING DEPARTMENT

DTRC ISSUES THREE TYPES OF REPORTS:

1. **DTRC reports, a formal series,** contain information of permanent technical value. They carry a consecutive numerical identification regardless of their classification or the originating department.

2. **Departmental reports, a semiformal series,** contain information of a preliminary, temporary, or proprietary nature or of limited interest or significance. They carry a departmental alphanumerical identification.

3. **Technical memoranda, an informal series,** contain technical documentation of limited use and interest. They are primarily working papers intended for internal use. They carry an identifying number which indicates their type and the numerical code of the originating department. Any distribution outside DTRC must be approved by the head of the originating department on a case-by-case basis.

NDW-DTNSRDC 5602-51 (Rev 2-88)

REPORT DOCUMENTATION PAGE

1a. REPORT SECURITY CLASSIFICATION: Unclassified	1b. RESTRICTIVE MARKINGS
2a. SECURITY CLASSIFICATION AUTHORITY	3. DISTRIBUTION/AVAILABILITY OF REPORT: Approved for public release; distribution is unlimited.
2b. DECLASSIFICATION/DOWNGRADING SCHEDULE	
4. PERFORMING ORGANIZATION REPORT NUMBER(S): DTRC–SME–89/76	5. MONITORING ORGANIZATION REPORT NUMBER(S)
6a. NAME OF PERFORMING ORGANIZATION: David Taylor Research Center; 6b. OFFICE SYMBOL (If applicable): Code 2813	7a. NAME OF MONITORING ORGANIZATION
6c. ADDRESS (City, State, and ZIP Code): Annapolis, MD 21402	7b. ADDRESS (City, State, and ZIP Code)
8a. NAME OF FUNDING/SPONSORING ORGANIZATION; 8b. OFFICE SYMBOL (If applicable)	9. PROCUREMENT INSTRUMENT IDENTIFICATION NUMBER
8c. ADDRESS (City, State, and ZIP Code)	10. SOURCE OF FUNDING NUMBERS: PROGRAM ELEMENT NO. 1–2813–959; PROJECT NO.; TASK NO.; WORK UNIT ACCESSION NO.

11. TITLE (Include Security Classification)
Electrochemical Impedance of Organic Coated Steel; Final Report—Correlation of Impedance Parameters with Long–Term Coating Performance

12. PERSONAL AUTHOR(S)
John N. Murray and Harvey P. Hack

13a. TYPE OF REPORT	13b. TIME COVERED	14. DATE OF REPORT (YEAR, MONTH, DAY)	15. PAGE COUNT
Research & Development	FROM_____TO_____	September 1990	47

16. SUPPLEMENTARY NOTATION

17. COSATI CODES			18. SUBJECT TERMS (Continue on reverse if necessary and identify by block number)
FIELD	GROUP	SUB–GROUP	Electrochemical impedance spectroscopy, Epoxy-polyamide coatings, Topcoat primers

19. ABSTRACT (Continue on reverse if necessary and identify by block number)

This final report presents a general overview of the use of Electrochemical Impedance Spectroscopy (EIS) as it applies to the evaluation of organic coated steels exposed to aerated, artificial (ASTM) sea water. The testing was performed over roughly a 6-year span with some samples subjected to immersion testing for up to 4 years. Three project reports have been previously issued covering: (a) the initial test efforts, (b) a summary style literature search on the use of EIS and coated metals, and (c) an experimental correlation of the EIS parameters with the first 550 days of sample exposure in ASTM sea water. The data from the latter report have been critically reviewed, supplemented with data from the continued testing of the same sample set and have been reanalyzed using a modified equivalent electrical circuit.

The testing involved four distinct types of epoxy-polyamide coatings dip-coated onto 1010 carbon steel panels. The two opaque types were primers and topcoat-primers per MIL-P-24441. Two transparent types involved a neat epoxy-polyamide coating with chemistry equivalent to that for MIL-P-24441 and the neat epoxy-polyamide system containing a silica filler. Each type allowed somewhat distinct observations with respect to coating deterioration and EIS parameter correlations.

The test program has demonstrated the capability of the EIS technique in assessing both the initial integrity of a coating system and in monitoring the coating degradation process. The data indicate EIS parameters allow identification of subfilm disbondment long before surface evidence of coating deterioration is apparent. The equivalent circuit model suggests disbondment areas as small as 0.0001% can be measured.

20. DISTRIBUTION/AVAILABILITY OF ABSTRACT	21. ABSTRACT SECURITY CLASSIFICATION	
☐ UNCLASSIFIED/UNLIMITED ☐ SAME AS RPT ☐ DTIC USERS	Unclassified	
22a. NAME OF RESPONSIBLE INDIVIDUAL: John N. Murray	22b. TELEPHONE (Include Area Code): (301)267-3151	22c. OFFICE SYMBOL: Code 2813

CONTENTS

TABLES

FIGURES

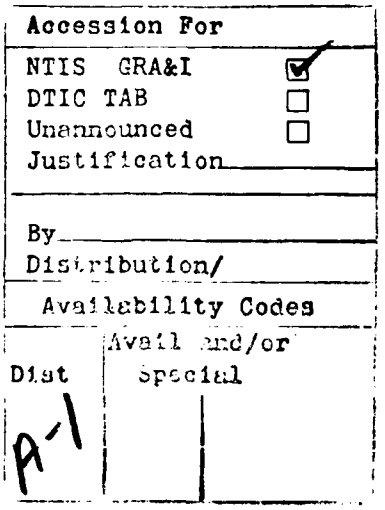

ABSTRACT

This final report presents a general overview of the use of Electrochemical Impedance Spectroscopy (EIS) as it applies to the evaluation of organic coated steels exposed to aerated, artificial (ASTM) sea water. The testing was performed over roughly a 6-year span with some samples subjected to immersion testing for up to 4 years. Three project reports have been previously issued covering the initial test efforts [1], a summary style literature search on the use of EIS and coated metals [2], and an experimental correlation of the EIS parameters with the first 550 days of sample exposure in ASTM sea water [3]. The data from the latter report have been critically reviewed, supplemented with data from the continued testing of the same sample set and have been reanalyzed using a modified equivalent electrical circuit [4].

The testing involved four distinct types of epoxy-polyamide coatings dip-coated onto 1010 carbon steel panels. The two opaque types were primers and topcoat-primers per MIL-P-24441. Two transparent types involved a neat epoxy-polyamide coating with chemistry equivalent to that for MIL-P-24441 and the neat epoxy-polyamide system containing a silica filler. Each type allowed somewhat distinct observations with respect to coating deterioration and EIS parameter correlations.

The test program has demonstrated the capability of the EIS technique in assessing both the initial integrity of a coating system and in monitoring the coating degradation process. The data indicate EIS parameters allow identification of subfilm disbondment long before surface evidence of coating deterioration is apparent. The equivalent circuit model suggests disbondment areas as small as 0.0001% can be measured.

ADMINISTRATIVE INFORMATION

This project was supported by the DTRC Ship and Submarine Materials Block Program under the administration of DTRC Code 0015. The project coordinator is Mr. Ivan Caplan. The work was performed under Work Unit 1-2813-959 and satisfies milestone 95CR3/5. The work was conducted at DTRC in the Marine Corrosion Branch, Code 2813, Mr. Robert J. Ferrara, Branch Head.

INTRODUCTION

Electrochemical Impedance Spectroscopy (EIS) has been shown by several investigators to be quite useful in monitoring changes to organic polymer coated metals when exposed to a variety of environments [5-9]. The EIS technique normally involves the use of the usual three electrode (test, counter and reference), electrochemical cell assembly. Applying a small magnitude a-c signal to the test and counter electrodes, one can measure the test electrode impedance and phase shift values over a reasonably wide range of a-c frequencies.

These data are then interpreted based on a variety of equivalent electrical circuit models. The organic coating itself exhibits capacitive (C_{coat}) behavior normally observed in the high frequency (10^3-10^5 Hz) range. If the metal becomes exposed to the electrolyte through flaws (holidays) or a general breakdown of the protective organic coating, corrosion of the metal initiates and the metal solution interface responds as a resistor-capacitor (R-C) circuit. This R-C circuit is normally observed in a lower frequency region (10^{-3}-10^1 Hz). The resistive element (R_p) has been shown by several investigators

[e.g., 10] to be inversely proportional to the metallic corrosion current and is considered to be the polarization resistance, normally reported with units of resistance times area, i.e., ohm cm^2. The capacitive response should be expected from considering the metal-electrolyte phase/charge separation. The classical studies [11] using a clean mercury surface in aqueous electrolytes result in "double-layer" capacitance (C_{dl}) values of 20-30 $\mu F/cm^2$. However, for corroding practical metals such as steel, a considerably higher interfacial capacitance is measured. Stable specific "pseudocapacitance" (C_{pc}), values of 200 $\mu F/cm^2$ and surface roughnesses of 3.5 have been determined for steel in a neutral (Na_2SO_4) electrolyte [12]. (Surface roughness is a unitless ratio of the true, absolute surface area of an exposed sample to the simple planer geometric area of the sample. Values range from 1.03 to above 100 depending on the material and construction of the test sample.) In many cell designs, the EIS technique has allowed measurement of the solution resistance (R_Ω) between the reference and test electrode at very high frequencies, this being helpful in supporting supplemental testing such as Tafel slope determinations.

A common electrical circuit model applied to coated metal surfaces in electrolytes is shown as Fig. 1. In addition to the previously discussed elements of C_{coat}, C_{dl}, R_Ω and R_p, an additional resistor (R_{pore}) is shown, representing one or a collection of pores through the coating. The value of R_{pore} is usually much larger than that of R_Ω. The three more common, generalized EIS data presentation formats for the circuit are shown in Fig. 2. Figure 2a presents the data in the Nyquist format (also termed the Cole-Cole plot, the Argand plot or the complex plane plot) where the impedance values at each frequency are resolved into the real and imaginary terms. The model in Fig. 1 predicts two semicircles which intercept the real impedance axis at three points. As noted earlier, the high frequency semicircle (left in Fig. 2a), is associated with the coating with intercepts at R_Ω and R_{pore} plus R_Ω. The coating capacitance can be determined via Eq. (1) by utilizing the frequency at the maximum (f_{max} in Hz) of the semicircle and the arithmetic difference between the two resistance readings.

$$C_{coat} = \frac{1}{(2)(\pi)(f_{max})(R_{pore})} \qquad (1)$$

The values of the Faradaic R-C semicircle (at the right in Fig. 2a) are determined in a similar fashion. The Bode formats (Figs. 2b and 2c) are considered by some investigators to be more useful than the Nyquist format with the horizontal data "lines" or "shelves" associated with the three resistive elements and the capacitive elements being associated with the -1 sloped line segments.

Usually all five of the circuit elements can be determined with conventional EIS equipment but occasionally the cell resistance is not resolved at the more common upper frequency instrumentation limit of 10^5 Hz. One can monitor the state of the coating using the "coating resistance" (the sum of all three R terms), the metallic corrosion process (R_p), the pore resistance (R_{pore}) or the coating capacitance (C_{coat}). Leidheiser [13] attributes the initial use of the d-c resistance measurements for monitoring the corrosion of painted metal surfaces to J.K. Wirth (1939-1942). A general quantitative range for the electrical resistance of a good coating was shown[14] to be $>10^8$ ohm cm^2 whereas poor coatings were associated with measurements of $<10^6$ ohm cm^2. Good coatings did show [14] some time variation of the measured resistance, probably as a small number of pores developed and then, somehow, became plugged again. Poor coatings tended to exhibit a

continual decrease in resistance as might be expected with the development of both larger, and more, pores and an increase in reactive metal surface.

The use of EIS for determining the total impedance/resistance of the coated metal system usually requires measurements in the low frequency range (i.e., 10^{-2}-10^{-3} Hz) which necessitates more measurement time than would a higher frequency method. Examining the theoretical EIS response of the coated metal model, Haruyama et al. [8] identified several unique features of a higher frequency measurement which they named the break-point frequency, f_h. This "point" is shown in Fig. 2b. as the higher frequency R-C intercept on the Bode magnitude schematic redesignated as f_M hi or f_{45} and, as can be seen in Fig. 2c, also corresponds to where the phase shift crosses 45° (therefore the designation, f_{45}) as the EIS response changes from that of the coating capacitance to the pore resistance. Their analysis showed f_{45} to be proportional to the area of the exposed metal as seen in Eq. (2), and to be independent of the coating thickness, hence a good monitor of the coating degradation process.

$$f_{45} = \frac{1}{(2)(\pi)(\varrho)(e)(e_o)} \frac{A_d}{A_t} \tag{2}$$

where ϱ is the pore electrolyte resistivity, e is the coating dielectric constant, e_o is the free space permitivity constant (8.85 X 10^{-12} V/m), A_d is the coating defect area and A_t is the total sample (coating) area.

The usefulness and holiday area proportionality to f_{45} was demonstrated in a soil corrosion experiment [15]. As will be shown, there are occasions where the break-point frequency can be determined from only the Bode magnitude data format. In these cases, the symbol f_M will be utilized to distinguish from break-point frequency measurements obtained off the Bode phase data format, f_{45}.

Earlier publications regarding this current study have examined the usefulness of the various EIS parameters in predicting the stability of coated epoxy coated steel samples submerged in ASTM sea water [1-3,16,17]. The long-term (550 day) visually assessed performance was shown to correlate with the change of total impedance, to the pore resistance and to f_{45}. The better correlation was obtained with EIS measurements obtained after 10-days exposure and was attributed to attaining some level of sodium ion diffusion through the coating to the metal surface [17]. Water and oxygen diffusion were considered to have occurred at significantly higher rates. The area relationship to f_{45} was noted to require a stable coating dielectric constant, a constant pore electrolyte resistivity or that the arithmetic product of these two terms remain constant. Possibly the changes of these two "constants" during the first 10 days of sample exposure could account for the lesser degree of correlation.

The general coated metal, equivalent circuit model was recently reexamined and the usefulness of a second, low frequency, break-point was observed [4]. The EIS spectra for the general coating model shown earlier in Fig. 1 was calculated for uniform cylindrical pores over an increasing pore area range of 0.000001% to 1%. The model (and its predecessors) also assumes the exposed metal area is the same as the coating pore area. The second, low frequency R-C network as noted earlier is associated with the polarization resistance (R_p) and the metal/electrolyte double layer capacitance (C_{dl}) or pseudocapacitance(C_{pc}). This second break-point frequency, now $f_{45\ lo}$, was evident with linear

dent of the pore area at $>10^{-3}$%. The Haruyama break-point frequency, now $f_{45\ hi}$, was seen to be a linear function of pore area in the range of >0.01%, detectable but nonlinear in the range of 10^{-4} to 10^{-3}% and becomes nondetectable at less than 10^{-4}%. A plot of the relationships of the two break frequencies with coating pore area is summarized as Fig. 3. As can be seen, $f_{45\ lo}$ would appear to be the better monitor for early, (i e., small percentages of pores) coating breakdown problems whereas $f_{45\ hi}$ would be applicable to the later stages of coating breakdown as well as to initially poor coatings.

There were two objectives for the present study. The first was to determine the utility of EIS measurements and equivalent circuit modeling in predicting long-term coating behavior from short-term data. The second objective was to establish a long-term EIS data base corresponding to the visually monitored coating breakdown and disbondment processes. Prediction is important for quickening coating reformulation testing and in quality assurance efforts. Acquiring long-term EIS performance data to enhance understanding of the coating degradation processes may provide important clues for additional coatings research.

EXPERIMENTAL

The experimental apparatus and EIS technique have been discussed in detail previously [1-3]. In general, four types of laboratory dip coated epoxies were applied to precleaned, 1010 carbon steel panels. These included different thicknesses of an epoxy polyamide primer per MIL-P-24441, a topcoat/primer epoxy polyamide system per MIL-P-24441, the neat (i. e., pure or unfilled) epoxy polyamide polymer coating with organic components per MIL-P-24441 and the neat epoxy system containing a high surface area silica filler. The latter two systems were transparent whereas the MIL-P-24441 coatings were opaque. Two electrical leads were added to one of the narrow sides of the coated sample and this area as well as the panel edges and back side was coated with a thick (~0.1 cm) protective layer of a commercial filled epoxy previously shown to be chemically stable in the aerated ASTM sea water used throughout the testing. The exposed coating area for the samples was roughly 7 by 9 cm. Although the protective layer was chemically stable, there was sufficient porosity to prohibit meaningful EIS measurements while the samples were undisturbed in the tank(s).

The samples were rack-positioned horizontally and submerged in aerated ASTM sea water for up to 4 years. Algae growth on the panels and tank surfaces occurred in long exposure tests and was minimized by adding an opaque coating to the tank top and walls. The ASTM sea water was continually aerated. Make-up deionized water was added when the level had decreased significantly and the solution was replaced roughly annually.

The majority of the samples was left in the natural condition. The potentials of these samples varied from positive values (vs. saturated calomel electrode, SCE), to the normal E_{corr} for unprotected steel under these conditions of -0.68 (+/- 0.02) volt, reflecting a tiny but undefined area of exposed steel. Two pairs of the topcoat/primer samples were subjected to cathodic protection potentials of -0.85 and -1.25 volt vs. SCE, respectively for the test period. Finally, a sample of each of the neat, the silica filled, and the topcoat/primer coatings was deliberately damaged using a special 0.08-cm-diameter tool and exposed in the natural E_{corr} condition.

Periodically, the samples were lifted from the tanks for EIS and visual performance evaluation. A thin layer of surface slimes was removed by a flowing cold tap water stream. The zone for the EIS clamp-on cell was pat-dried with a clean white paper towel. The O-ring sealed, clamp-on cell containing the counter electrode was then attached, fresh ASTM sea water added and the reference electrode positioned. The assembly would be essentially ready for EIS testing within roughly 5 minutes after removal from the tank. Visual estimations of the blistering and/or rusting were made at the same time with photographic documentation of the coating surfaces made roughly every 6 months. Quantitative valuations of the blistering/rusting were made via ASTM D-610/714 and have been reported previously [3, 17]. Area percentages have been redetermined from the sample photographs and these area values are utilized in this report.

The EIS data were obtained utilizing a Stonehart BC-1200 potentiostat, a Solartron 1250 Frequency Response Analyzer controlled by a Tektronix 4052 computer. In most cases, a 1000 ohm measuring resistor was utilized. With an input signal of 60 mV to the 13.1 cm^2 sample area defined by the test cell area, this would result in an upper impedance measuring limit of 5 X 10^7 ohm cm^2. Highly stable and resistive coatings have been tested without damage using a 500 mV signal resulting in a higher measuring limit of 2.5 X 10^8 ohm cm^2. In general, large signals should be avoided as visual rusting has been accelerated in poor coatings when using only a 10 mV signal. The use of a higher resistance measuring resistor, which would also raise the measurement limit in the low frequency range, adversely affected the high frequency data and therefore was discontinued after a few trial runs. Instrumental functionality and accuracy checks were made periodically using electronic component "dummy cells" assembled with 1 or 2% precision components.

Analysis of the EIS data was made utilizing the assumptions of the basic equivalent circuit shown previously in Fig. 1. As suggested earlier, the cell resistances could not be measured with the upper frequency limit of 65,500 Hz of the equipment. For the other components, both Bode and Nyquist format graphs were used to extrapolate or interpolate values to allow calculations of the two capacitances and the three resistor values. For C_{coat}, the interpolated impedance measured on the Bode magnitude plot at 10^4 Hz was used with Eq. (1.) The capacitive slope would be adjusted to -1 for some improvement in accuracy, the normal measured slope being between -0.97 and -0.99. Identifying the presence of a narrow frequency range, impedance "shelf" corresponding to R_{pore} in the Bode magnitude format was assisted in many cases by the Bode phase information. The frequency of the minimum value of the phase response would be utilized to verify if a small impedance "shelf" was present in the Bode magnitude data format. The C_{dl} value (or C_{pc}) was normally calculated from the Bode magnitude and phase plot information using Eq. (3.)

$$C_{dl} = \frac{1}{(2)(\pi)(f_{pm})(R_p)} \sqrt{1 + \frac{R_p}{R_{pore}}} \qquad (3)$$

where f_{pm} is the frequency of the phase minimum and the other terms are as given previously.

The polarization resistance (R_p) was normally interpolated from the Bode magnitude data format. The coating resistance/impedance, the sum of the electrochemical resistances, was taken as the maximum value (R_{max}) observed, usually at 10^{-3} Hz. Occasionally the

EIS spectra suggested R_{max} to be essentially a diffusional impedance and therefore to be probably somewhat less than would be determined in a "pure" d-c measurement. The values were quite high and therefore should be considered as another indication of a good, but not great coating.

RESULTS AND DISCUSSION

The results from the study are presented in three sections: visual blister area assessment, the use of initial EIS parameters in predicting long-term coating performance and the use of the EIS parameters in monitoring the coating delamination process over time. The results are then also subgrouped in the last two sections by the parameter of interest from the EIS spectra. Within each of these sections, data are discussed as they relate to the four material types: (1) The primer coating data from four distinct coating thicknesses allowed time trends to be determined. (2) The transparent coatings allowed direct observation of subfilm events which did not necessarily result in blistering as defined by an apparent rise in the coating surface. (3) The opaque topcoat/primer system is the major system of interest and (4) The last group is that involved in determining the effects of different cathodic potentials on the delamination process.

BLISTER AREA ASSESSMENT

The delamination process or blistering data from the various epoxy coating systems are summarized in Figs. 4, 5 and 6 for the primer samples, the other coatings and the cathodically protected samples, respectively. As can be seen, once the process starts, the delaminating area tends to increase linearly with exposure time. This is as expected from diffusional considerations where the diffusing front (linear distance) would increase with the square root of time. Since blister area increases as the square of the diffusion front, this results in a linear area-time relationship. This general behavior has been observed with polybutadiene and alkyd coatings [18] on steel and adhesive bonded rubber on steel [19].

The onset/delay time and the rate data for the four classes of coatings are also summarized in Tables 1 through 4. Although there may be a relationship between the coating thickness and either the onset time or the blistering rate, the type of coating (filled vs. neat) is seen to be more influential. Whereas the filled polymer coatings exhibited roughly a 10% per year blistering rate, the neat system degraded at a ten-fold higher pace. Additionally, in the primer series, the thinner coatings were one layer (dip) samples whereas the two thicker pairs were two layer coatings with roughly a week, room temperature, cure time between applications. The dual layer structures were significantly superior with respect to the onset time.

The reported "blistering" rates for the transparent coatings may also be higher as a result of being able to observe delaminations, (i.e., subfilm patterns, as opposed to general discolorations) which might not affect the surface topography sufficiently to be considered as an "ASTM blister" in an opaque coating. These transparent coating delamination rate data should however be more applicable to rate data obtained via the EIS technique. A question as to a uniformly discolored subfilm surface being considered as disbonded and therefore the coating not exhibiting the "standard" dielectric constant was not resolved. An easily observed, mosaic/pattern was considered necessary to rule that area as disbonded.

The applied potential also influences the topcoat/primer blistering rate as can be seen in comparing the data in Table 4 to that of Table 3. The more cathodic potential clearly accelerates both the onset time and the blistering rate.

THE USE OF INITIAL EIS PARAMETERS IN PREDICTING LONG-TERM COATING PERFORMANCE

The initial EIS parameter values are summarized in Tables 5 to 8. Although several of the EIS runs were made within 1 to 2 hours of ASTM sea water exposure and therefore are truly "initial runs", a few samples were evaluated as late as 7 days following exposure. The day after immersion of the initial EIS run is included as part of the sample number in Tables 5 to 8.

Coating and Metal Polarization Resistance, R_{max} or R_p

The only initial EIS parameter found to correlate with the visual epoxy coating blistering/degradation processes is the coating resistance R_{max} (as well as the corresponding metallic corrosion R_p). As suggested in the introduction, when R_{max} exceeded 10^8 ohm cm^2, the coating performance was good or excellent. If the value was less than 10^6 ohm cm^2 then the coating performance was poor. Applying a cathodic potential for as short as two days lowered the initial 10^8 R_{max} value to about 3×10^7 ohm cm^2, the blistering rate was then dependent on the level of applied cathodic potential .

In that the coating resistance is a measure of the electrochemical processes transpiring through the coating, one should expect both visual blister parameters to be related to the coating resistance. Just as the polarization resistance is inversely proportional to the corrosion current density via the Stern-Geary equation, the coating resistance value can also be equated with an electrochemical rate or current density. Higher R_{max} values should represent superior barriers for corrosion processes and therefore should be directly proportional to the blister onset time. This premise is not inconsistent with the data as can be seen in Fig. 7. The set of four thinner primer samples which exhibited degradation on immersion into the ASTM sea water have been arbitrarily positioned at 0.1 day, and the four samples showing no blistering at the time of this report are shown at the right of the data field as indicated with arrows. The scatter is large as the data represent different materials as well as number of coats in the case of the primer system. Once the blistering process has initiated, the blister area expansion rate should be directly proportional to the corroding processes, and therefore inversely proportional to the R_{max} value. The correlation should be best for the value of R_{max} at the time of the blister propagation but a reasonable correlation to the initial R_{max} values of at least the primer coatings is also observed in Fig. 8 where the data are plotted on a log-log basis. Again, the scatter for the other materials and test conditions is apparent but the general behavior is what one would expect.

The primer coatings, R_{max} data show a bimodal correlation with coating thickness, the one coat samples with a calculated specific resistivity of 5×10^8 ohm cm and the dual coating pieces with the significantly higher value of 2×10^{10} ohm cm. This may be another confirmation of Mayne's argument [20] that a second layer with a given distribution of flaws has a low probability of site matching to the first layer. The three neat polymer samples exhibited the highest average specific resistivity of 3.4×10^{10} ohm cm, whereas the dual coated, filled samples all averaged about 2×10^{10} ohm cm. These

values are significantly below the reported [21] volume resistivity range for cast epoxies of 10^{16} to 10^{17} ohm cm. This is caused by the thru-film flaws (pores) which are electrochemically conductive, as well as because of the EIS instrumentation limitations.

There is insufficient evidence to support a closer relationship between initial R^{max} values in the 10^8 range with either the onset time or the blistering rate that is independent of the type of material. This can be seen in the wide range of visual blistering data between the neat coatings and the topcoat/primer systems while the initial R_{max} values are all from 2 to 4 x 10^8 ohm cm^2.

Coating Pore Resistance, R_{pore}

The presence of a measurable R_{pore} shelf correlates to a certain extent with the blistering onset time with the more stable coatings tending to have no discernable shelf in the Bode magnitude data format and no inflection in the Bode phase format. The equivalent circuit model would suggest that a C_{dl} value about the same as C_{coat} would be required to enable R_{pore} to be measurable. This would be expected to take some time (days?) to develop. The thinner primer samples with R_{pore} values less than 10^4 ohm cm^2 exhibited considerable corrosion from the initial submerge time.

Coating Capacitance, C_{coat}

The initial coating capacitance values from the EIS technique showed no particular relationship to the coating stability but did, as expected, show the inverse relationship with thickness. Excluding the 20-μm-thick primer samples, the capacitance values corresponded to a dielectric coefficient (e) of 3.7, acceptably close to the 3.6 value for cast epoxies [21]. The addition of mineral fillers could raise the initial (and dehydrated, i.e., water free) e value to the 4-8 range depending of the particular materials involved. The significantly higher values observed with the 20-μm-thick primers might reflect rapid absorption of water but are probably more associated with data deconvolution problems with these samples with relatively close R_{pore} and RΩ values.

Break-Point Frequencies, $f_{45\ hi}$ (or f_{45}), $f_{M\ hi}$ (or f_M), $f_{45\ lo}$, $f_{M\ lo}$

Discussion of the usefulness of the initial break-point frequencies requires the determination of which break-point frequency is displayed. No, or very low values, are associated with good coatings (i.e., long blister onset times) as the data in Tables 5 through 8 indicate. In several cases and especially with the thinner primer coatings, the more cleanly defined data for the low break-point frequency value would be available only from the Bode phase data format. The maximum phase shift value would be less than 40° and therefore a true $f_{45\ lo}$ value could not be determined. Rather than disregard the information, the frequency at the "phase-wave" half height, designated as $f_{45\ lo}$, was utilized, these values then included in the tables.

Based on the equivalent circuit model, the low (i.e., less than 1 Hz) frequencies would indicate a corrosion area of less than 0.0001%. This would suggest the break-point frequency can be used to monitor the onset of the blistering considerably before any visual evidence is apparent. The presence/values of initial higher break-point frequencies does not correlate with the observed blistering rate.

THE USE OF EIS PARAMETERS IN MONITORING COATING PERFORMANCE OVER TIME

Coating and Metal Polarization Resistances, R_{max} or R_p

The coating resistance (R_{max}) or the polarization resistance (R_p) both correlate quite well with the disbonded areas for samples showing rapid development of visual rust and/or blisters. The value of R_p is normally between 60 and 95% of R_{max} depending on the extent of coating damage and the magnitude of R_{pore}. By using a Stern-Geary constant of 0.0174 (60 mV anodic, 120 mV cathodic Tafel constants) and assuming the steel corrodes at a 1 $\mu A/cm^2$ rate, the calculated corroding area values match the visual rust/blister area data with respect to time for the 20 and 55-μm-thick primer coatings when the exposed areas are in the 15 to 80% range as is shown in Figs. 9 through 12. The ASTM rust area values, previously applied as an equivalent blister scale, are included on the figures as an additional reference. In the exposed area range of about 5 to 15%, the use of a 0.03 $\mu A/cm^2$ corrosion current density would allow an excellent fit as can be envisioned in Fig. 12. This lower corrosion current density also yielded good disbonded area values when used for the one thicker (121 μm) primer coating which exhibited blistering as is shown in Fig. 13. As can be seen, the R_p data track the visual blister areas quite well.

The three thicker primer coatings showing no blistering (116, 180 and 183m), exhibited the same general changes of an early decrease in R_p, possibly indicating 0.01% disbondment, and then slowly increased to the 10^8 ohm cm^2 range. This general behavior also occurred with the two topcoat/primer samples not exhibiting rust/blisters in the 3.5+ years exposure.

The R_{max} and R_p values did not track well with samples showing long blister onset times which also coincide with nonrusting blisters. The initial values were high (10^8 ohm cm^2) and either remained high or became somewhat higher with time. This was observed with one topcoat/primer sample and the neat as well as silica filled clear epoxies. Final blister areas varied from 5 to 85% and neither R_{max} nor R_p values give an indication of the beginning or development of this blistering process. A typical data set is presented in Fig. 14, the data being from the 74-μm- thick neat epoxy coating. Lowering the corrosion current density to $0.01 A/cm^2$ for the R_p area calculations shows an apparent initiation of the disbonding in the first 9 or so months, this corrosion current then falling and staying low after about 15-months exposure. One explanation for this rather dramatic contradiction to the behavior of the primers would be that the pore resistances were large and beyond the range of this particular instrumental setup and therefore the changes to the coating impedance values were not observable. In addition, the conductive region(s) of the coating may have been located adjacent to the cell area. The coating in the cell area may have been truly resistive preventing electrochemical communication with the subfilm metallic surface. Therefore the presence of a high R_{max} or R_p value did not assure subfilm inactivity whereas a moderate value would assure activity.

Coating Pore Resistance, R_{pore}

As mentioned earlier, the presence of a measurable R_{pore} tended to mean that the corrosion process was reasonably active. If, however, the metallic pseudocapacitance was less than about 150% of the coating capacitance, then R_{pore} would not appear as a cleanly identified "shelf" in the Bode data format. This tends to rule out the use of R_{pore} to moni-

tor the early disbonding process except with rapidly degrading coatings. In those cases the R_{pore} values decreased at the rate predicted by the equivalent circuit model. There seems to be a divergence of measured R_{pore} values compared to model numbers at smaller pore areas, with the measured R_{pore} values becoming significantly larger than expected. This might be explained by utilizing a different calculation for the small pore resistances which has been derived for porous insulators as used in battery/fuel cell separators [22].. The increase in the electrolyte resistivity caused by the porous coating (separator) is related to the normal geometric factors, increased by volume quantity of the solids. The relationship for a porous body of cylindrical particles is given as Eq. (4) and shows that where solids contents exceed 99%, this factor dominates the resistance calculation.

$$R_{separator} = \frac{\varrho \quad (\quad \cdot \quad)}{A(1-f)} \tag{4}$$

where ρ is the electrolyte specific resistivity, l is the pore length or coating thickness,A is the coating area and f is the solids volume fraction.

This relationship has been shown [22] to be influenced by the general particle shape, therefore by the general configuration of the pore, and has been verified experimentally for the density range of 10 to 95%.

Coating Capacitance, C_{coat}

The coating capacitance values increased with exposure time in an expected exponential fashion. Typical data are shown in Fig. 15 for the topcoat plus primer samples. The increase in coating capacitance would correspond to the increase in dielectric constant by water absorption of from 3 to 5 weight percent. The effect on the dielectric constant of exchanging residual coating solvents (i.e., 2-ethoxy ethanol, 2-butoxy ethanol and mineral spirits paint thinner) in the coating with water is unknown.

The thinner, most rapidly corroding primer samples decreased in impedances to a sufficient extent that the only measurable capacitance was that of the metallic surface, the coating capacitance would be measurable only above 65 kHz.

There may be a tendency to observe a slight decrease in coating capacitance with the samples showing the longer blister onset times. This would be expected via a loss of coated area. However, the data did not support as large an area change as was observed visually. A reevaluation of the basic coating equivalent circuit model is necessary for further insight into this problem.

The coating capacitance values should provide interesting information with respect to influx of water and changes to the chemistry of the polymer with continual exposure time. However, as the value is a function of three factors: (area (perhaps bonded and non-bonded); film thickness; and dielectric constant) all of which may be changing with continued exposure time, this EIS parameter does not appear suitable to monitor disbonding area.

High Break-Point Frequency, $f_{45\ hi}$ (or f_{45}), $f_{M\ hi}$ (or f_M)

The high break-point frequencies tend to correlate in a similar fashion as the R_{max} values. As seen in Figs. 16 through 19, the $f_{M\ hi}$ values for the thinner primers increased at a 1 kHz/% active area rate, considerably lower than the model parameters predicted (~4000 kHz/%). This 1 kHz/% parameter was used to calculate disbondment area values

and these were included in Figs. 9 through 14 where the area fits were presented on a linear and time basis. There was an upper applied frequency limit via the instrumentation of 65.5 kHz which therefore limited the higher area percentages to the 50% range. The high break-point frequency tended to track at a constant value in the 1 to 15% range as the model would suggest. The value from the Bode magnitude data format ($f_{M\ hi}$) was, in general, easier to evaluate than the Bode phase (f_{45}) information. The f_{45} values could be masked by both the sample exhibiting low impedance values leading to overall phase shifts less than 40 degrees as well as resolution interferences from the low frequency break-point frequency process.

The high break-point frequency values for the samples showing no blistering tended to decrease with sample exposure time. Typical results from the 180-μm-thick primer are presented as Fig. 20. Using the 1 kHz/% value, the data would suggest exposure areas could be as high as 10% initially but decrease to less than 1% within 6 months. Initial subfilm delamination area values this large that do not result in visual coating damage appear illogical and suggest a closer reexamination of the model parameters is in order.

The six samples which developed delamination/blisters after the longer onset times all tended to show an initial high constant and then increasing f_M value during the first 9 or so months exposure. In two cases the increase tracked with the appearance and an increase in delamination/blister area, the data for the 69-μm neat epoxy coating presented in Fig. 21. In four cases the f_M value decreased sharply at about 1-year exposure and remained low with the blisters developing at 2.4 to 3.5 years exposure, a typical data set shown in Fig. 22 for the 157-μm- thick topcoat plus primer sample. Samples showing blistering after 2-years exposure did not exhibit a positive correlation with f_M values around or following the observation of the physical blister. In that five of these six samples were transparent and the initial definition of delamination required a mosaic or pattern, perhaps the presence of the uniform discoloration by itself was sufficient to result in an electrochemically active surface. The model parameters for this situation have not been resolved at this time.

Low Break-Point Frequency, $f_{M\ lo}$ or $f_{45\ lo}$

The model calculations suggested that the low frequency intercept between the metal surface capacitance slope and R_p, would be more useful with small delamination areas. A value of between 0.1 and 1 Hz (with R_p levels of 10^5 ohm cm^2) was normally observed for the highly corroding samples as is shown in Figs. 16 and 17 and the value would remain roughly constant throughout the test. The model suggests a constant upper limit of 6 Hz for delamination areas above 10^{-3}%; therefore, the observations were somewhat consistent with the model.

However, the samples showing no delamination also exhibited a constant $f_{45\ lo}$ value in the 0.01 to 10 Hz range, a typical set of results being shown in Fig. 20. The general EIS spectra for these samples, especially in the later stages, could be described as largely capacitive with a upper, high, perhaps instrumental measurement limit shelf (which might be misinterpreted as R_{max}). Again, a more sensitive unit allowing higher impedance measurements in the 10^{10} to 10^{12} ohm cm^2 range appears to be required for using $f_{M\ lo}$ as the area monitor in the early delamination stages.

SUMMARY

Epoxy coated steel samples were exposed to ASTM sea water for up to 4 years and monitored using EIS and visual techniques for determining coating delamination rates. The EIS parameters were shown to be quite useful in the study of coating delamination/ degradation processes. The following specifics were noted:

- EIS is most useful when the coating degrades, opening pores as the degradation progresses. Then R_{max}, R_p, R_{pore}, and f_M or f_{45} can be used to identify disbonded areas as well as the rate of disbonding. The thin, single coat, primer samples served as good examples here.
- Of the EIS parameters, R_{max} or R_p appear to be the most useful as they allow an initial appraisal of the coating integrity. Then R_{max} or R_p can be used to monitor changes to the film as environmental exposure is continued.
- EIS parameters allow "observation" of subfilm delamination processes prior to surface topography changes.
- EIS is also useful for monitoring the case of visually observed blistering which has an apparent, limited pore area.
- Different model parameters are apparently needed when coating pores plug but the blister area continues to grow. Here, the true area of disbondment may be quite high but the EIS spectra is controlled by R_{pore}. The metallic area may have a considerably lower corrosion rate as the alkalinity of blister liquor increases. C_{pc} and or C_{dl} may be significantly different in the alkaline fluid vs ASTM sea water. It is possible that nothing in the EIS spectra would be proportional to disbonded area during the transition period between the three possible models.
- The use of the high Hz break-point frequencies, f_{45} or $f_{M\ hi}$ appears to be limited to monitoring delamination areas of from 1 to about 75%. The current model would suggest the f_{45} value should be applicable for monitoring down to a lower delamination area of 0.01%. However, the epoxy coated samples showed that the metal surface pseudocapacitance causes an interference in the approximate range of 0.01 to 1% delaminated area.
- The coating capacitance (C_{coat}) value which was readily determined is not appropriate for monitoring delamination areas. The change in C_{coat} value during the first 100 or so hours may be related to blister propagation rates, however there was insufficient data in this experiment to determine a relationship. Further investigation is warranted in this area.
- The low break-point frequency, identified in a reanalysis of the coating equivalent circuit model, should be applicable for monitoring the delamination area during the initial periods of the coating delamination processes. The instrumentation and test cell require improvement to allow measurement of coating impedances of 10^{12} ohm cm^2 for a meaningful use of $f_{M\ lo}$.

CONCLUSIONS

The utility of EIS for predicting long-term coating performance from short-term data has been verified. To this end, specific EIS parameters and their utility and limitations have been identified. EIS also has utility in following coating degradation over time. There are, however, some issues to be resolved regarding correlation of certain EIS parameters with coating degradation processes. The usefulness of $f_{M\ lo}$ in monitoring the initiation of the delamination process and the modeling of rustless blister formation are two areas of immediate interest.

ACKNOWLEDGMENTS

This project was initiated and monitored by Dr. John R. Scully during the period of 1985-1988 [1-3]. The coated samples were prepared by Drs. George Loeb and Jim Mihm. Bryan Pearce provided technician support throughout the 4-year effort.

Table 1. Disbonding rate data for primers via ASTM D--610/714.
(cell area only)

Sample Number	Coating Thickness (μm)	Onset Delay (days)	Disbonding Rate, ASTM (%/day)
406	20.0	0	0.7
407	24.6	0	0.37
401	54.2	0	0.027
402	55.0	0	0.037
332	116.0	1095	~0.005
331	120.8	185	0.026
327	180.3	>1460	0
326	182.9	<1460	0

Table 2. Disbonding rate data for transparent coatings via ASTM D-610/714.
(cell area only)

	Sample Number	Coating Thickness (μm)	Onset Delay (days)	Disbonding Rate; ASTM (%/day)
Neat	201	68.3	930	0.19
	202	69.4	220	0.26
	206	73.9	140	0.16
Plus Silica	101	75.9	1240 est.	0.04 est.
	102	77.0	870	0.037

Table 3. Disbonding rate data for topcoat/primers via ASTM D-610/714.
(cell area only)

Sample Number	Coating Thickness (μm)	Onset Delay (days)	Disbonding Rate; ASTM (% day)
318	146.5	>1210	0
317	156.9	845	0.012
316	159.7	>1330	0

Table 4. Disbonding rate data for potential affected coatings via ASTM D-610/714. (cell area only) (H indicates 0.007 cm^2 holiday)

	Sample Number	Coating Thickness (μm)	Onset Delay (days)	Disbonding Rate; ASTM (%/day)
Neat	205H	74.8	~9	~1.0
Plus Silica	105H	84.1	~45	~0.022
Topcoat/Primer	325H	143.4	<23	~0.020
Topcoat/Primer, -0.85V	319	145.3	>1189	0
Topcoat/Primer. -0.85V	320	155.2	550	0.004
Topcoat/Primer, -1.25V	321	155.5	196	0.026
Topcoat/Primer, -1.25V	322	158.6	453	0.039

Table 5. Initial EIS parameters from epoxy primer coatings.

Sample Number	Coating Thickness (μm)	R_{max} (ohm cm^2)	$C_{coating}$ (pF/cm^2)	R_{pore} (ohm cm^2)	f_M (Hz)	f_{45} (Hz)
406,d-1	20.0	$5.0X10^4$	3625	5775	7160[a]	1180[b]
407,d-1	24.6	$1.4X10^4$	6155	604	44000[a]	?[d]
401,d-1	54.2	$6.1X10^5$	144	357000	2865[a]	4650[a]
402,d-1	55.0	$5.2X10^5$	177	178500	5020[a]	8400[a]
332,d-4	116.0	$5.2X10^7$	121	26500	40225[a]	14[a]
331,d-4	120.8	$5.8X10^6$	107	61690	25000[a]	134[c]
327,d-1	180.3	$1.3X10^8$	71	304000	6390[a]	6608[a]
326,d-3	182.9	$2.1X10^8$	101	26500	65000[a]	4[c]

a = High frequency intercept; b = estimate of 1/2 phase height; c = Low frequency intercept; d = not measurable.

Table 6. Initial EIS parameters from transparent coatings.

Sample Number	Coating Thickness (μm)	R_{max} (ohm cm^2)	$C_{coating}$ (pF/cm^2)	R_{pore} (ohm cm^2)	f_M (Hz)	f_{45} (Hz)
201, d-3	68.3	$3.6x10^7$	186	13125	65500	-
202,d-2	69.4	$4.4x10^8$	121	-	-	-
206,d-28	73.9	$2.4X10^8$	84	-	-	-
101,d-3	75.9	$2.7X10^8$	10	696000	22300	15725
102,d-3	77.0	$1.3X10^8$	10	$1X10^7$	1510	1500

Table 7. Initial EIS parameters from epoxy primer plus topcoat coatings.

Sample Number	Coating Thickness (μm)	R_{max} (ohm cm^2)	$C_{coating}$ (pF/cm^2)	R_{pore} (ohm cm^2)	f_M (Hz)	f_{45} (Hz)
318,d-1	146.5	$2.3X10^8$	85	-	10 (lo)	77 (lo)
317,d-6	156.9	$3.4X10^8$	31	88500	4 (lo)	13 (lo)
316,d-6	159.7	$3.3X10^8$	82	-	5 (lo)	2 (lo)

Table 8. Initial EIS parameters from potential affected coatings.

Sample Number	Coating Thickness (μm)	R_{max} (ohm cm^2)	$C_{coating}$ (pF/cm^2)	R_{pore} (ohm cm^2)	f_M (Hz)	f_{45} (Hz)
205,d-1	74.8	$7.4X10^7$	371	-	6.2 (lo)	5.3 (lo)
105,d-1	84.1	$1.3X10^8$	294	-	4.1 (lo)	0.1 (lo)
325,d-2	143.4	$3.7X10^8$	220	-	1.5 (lo)	0.1 (lo)
319,d-2	145.3	$3.8x10^7$	82.8	91500	$2.1X10^4$	156
320,d-2	155.2	$1.0X10^7$	87.6	109000	$1.7X10^4$	590
321,d-2	155.5	$11.5X10^7$	86.9	55000	$3.6X10^4$	831
322,d-2	158.6	$3.5X10^7$	85.4	-	53	462

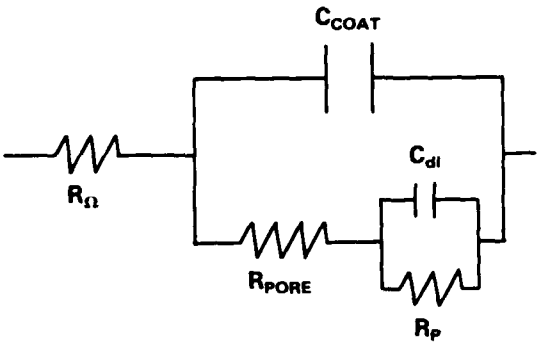

WHERE
C_{COAT} = COATING CAPACITANCE
C_{dl} = DOUBLE LAYER CAPACITANCE
R_Ω = SOLUTION RESISTANCE
R_{PORE} = COATING PORE RESISTANCE
R_P = METAL POLARIZATION RESISTANCE

Fig. 1. General electrical equivalent circuit model for coated metal surface.

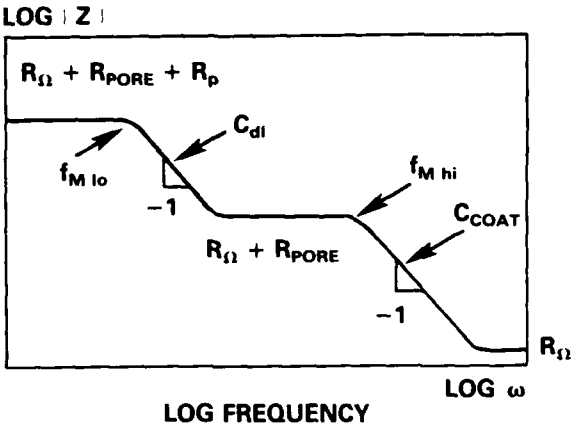

LOG FREQUENCY

(SYMBOLS SAME AS FIGURE 1,
$f_{M\ lo}$, $f_{M\ hi}$ BREAK-POINT FREQUENCIES)

Fig. 2b. Bode magnitude format.

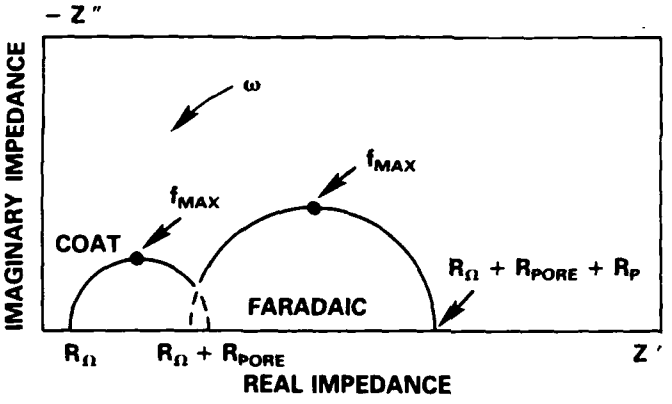

(SYMBOLS SAME AS FIGURE 1, ω = 2πf,
f = FREQUENCY (cy/sec), Z = IMPEDANCE)

Fig. 2a. EIS Nyquist format.

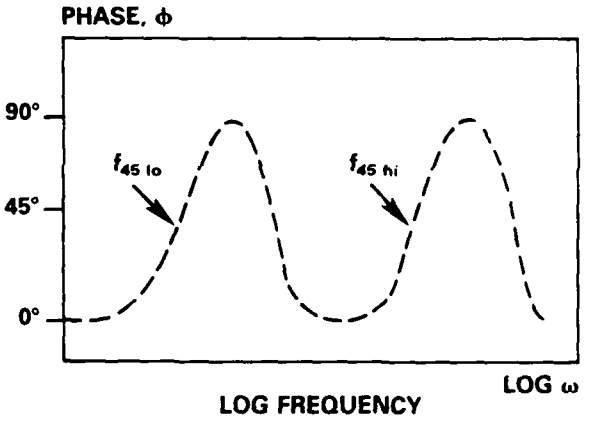

LOG FREQUENCY

(SYMBOLS SAME AS FIGURE 1,
$f_{M\ lo}$, $f_{M\ hi}$ BREAK-POINT FREQUENCIES)

Fig. 2c. Bode phase shift format.

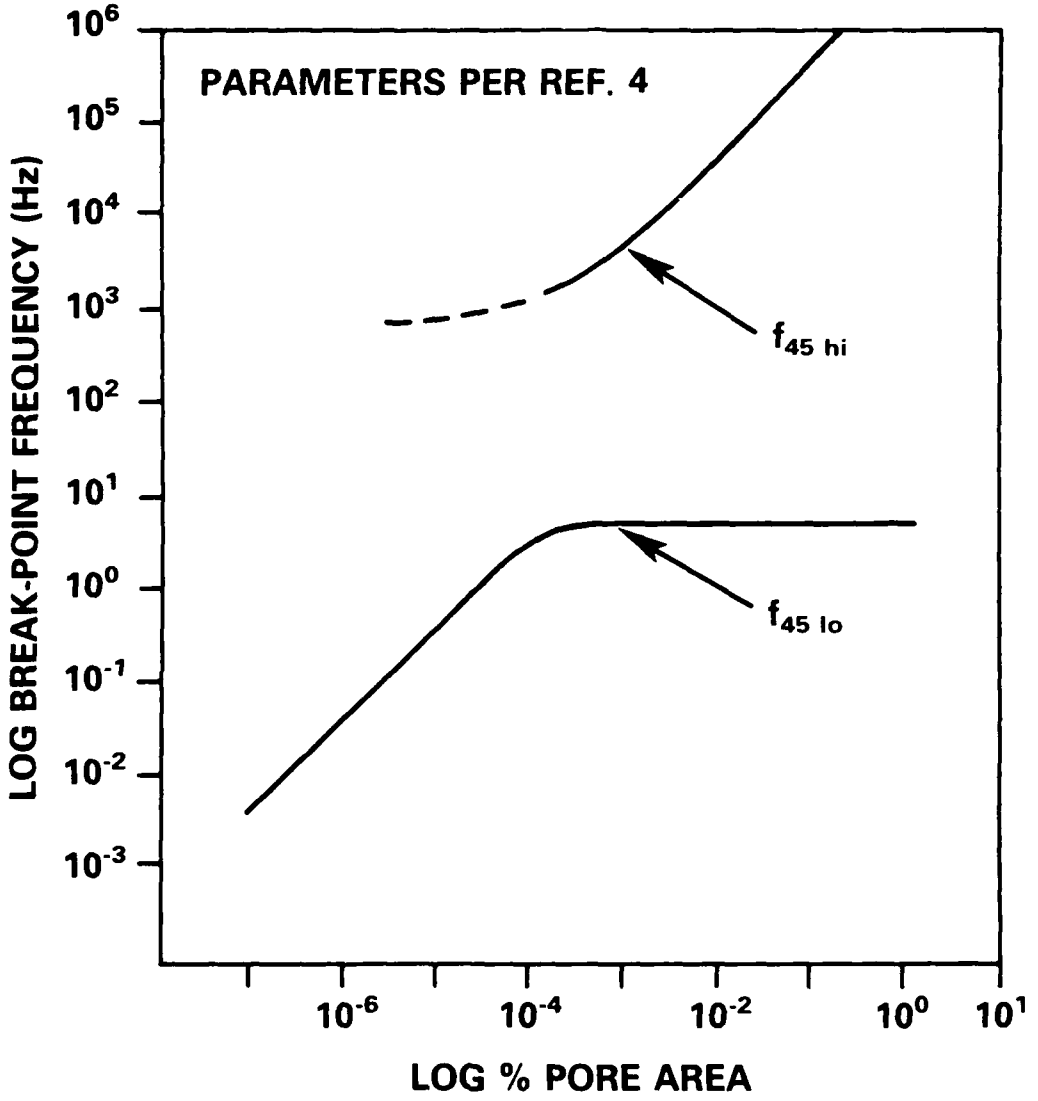

Fig. 3. Break-point frequencies as a function of pore area.

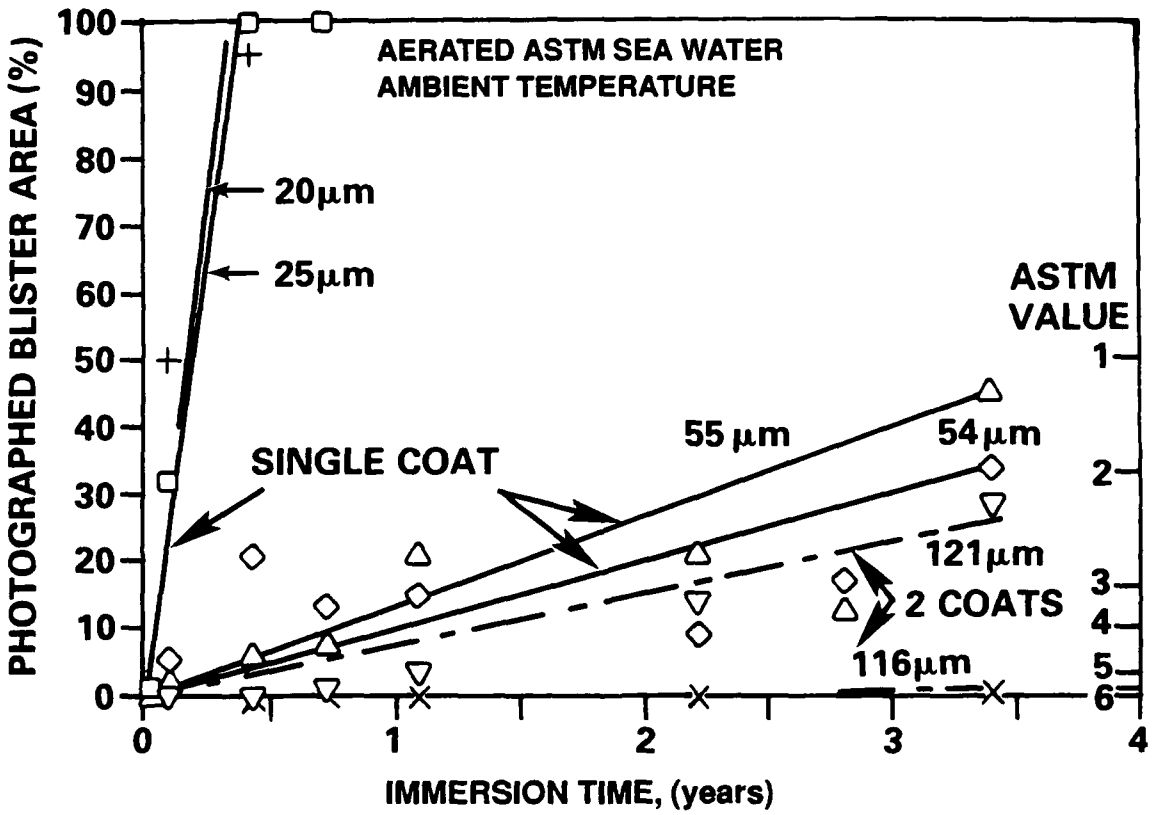

Fig. 4. Primer epoxy coating disbondment rate data.

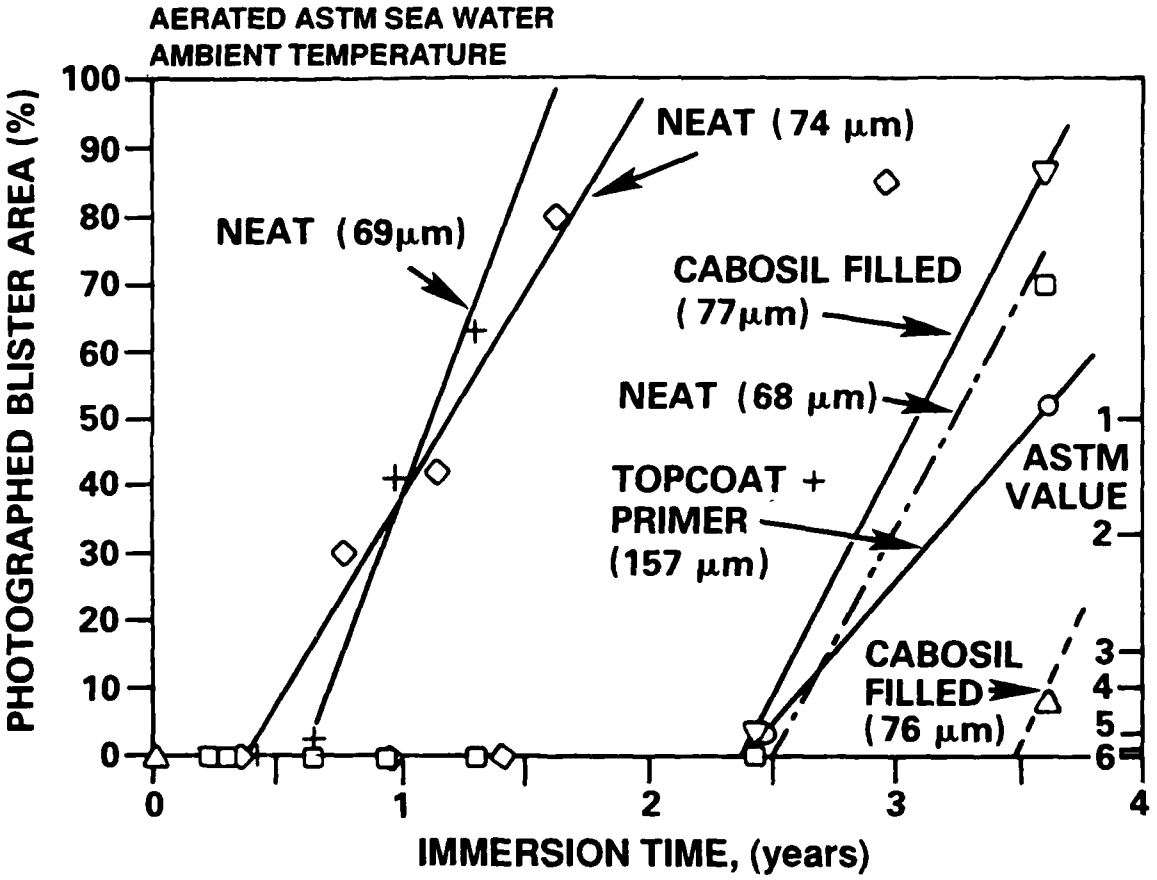

Fig. 5. Disbondment rate data for various epoxies.

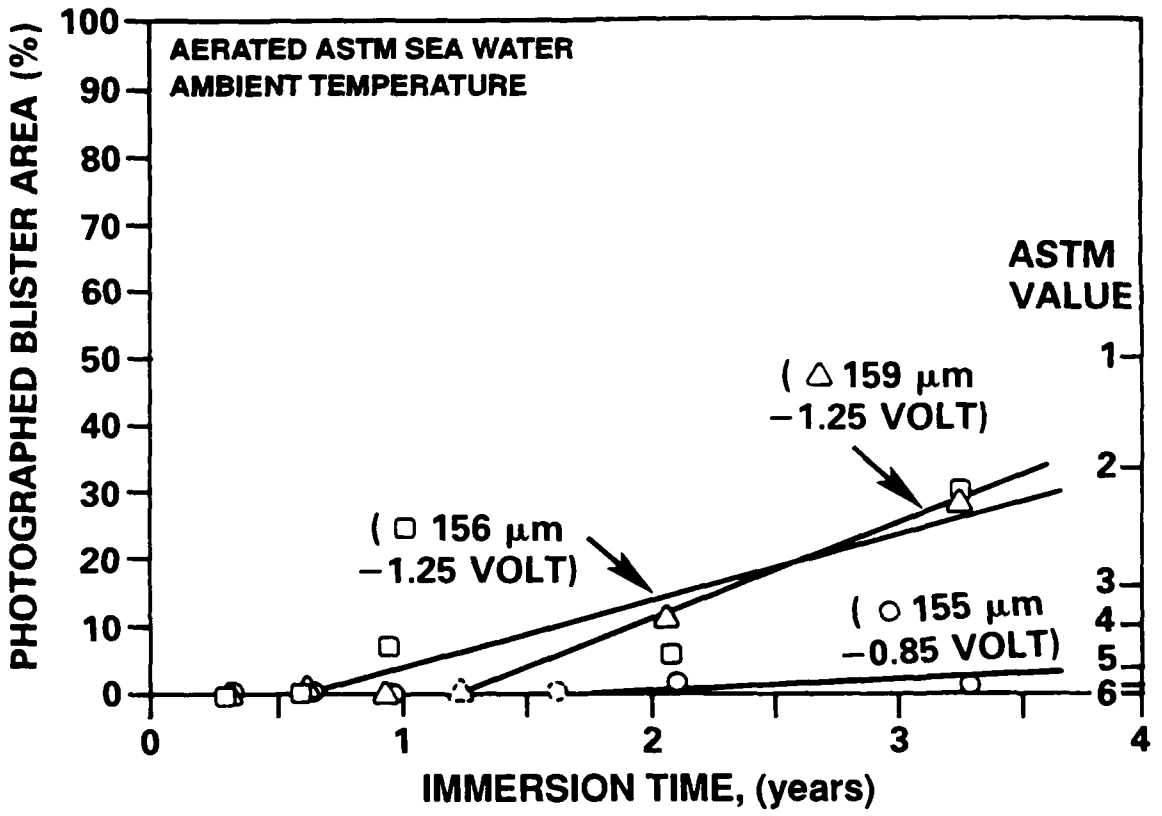

Fig. 6. Cathodic delamination of epoxy coatings.

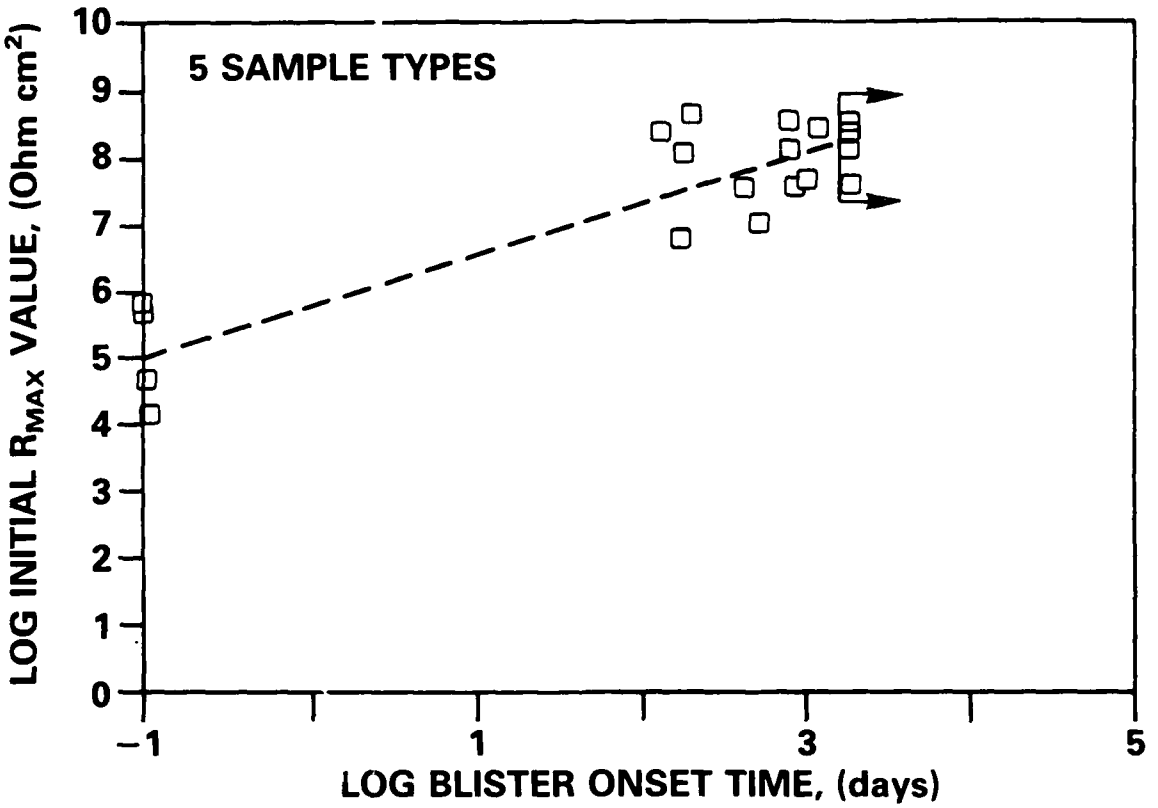

Fig. 7. Initial R_{MAX} data and blister onset time.

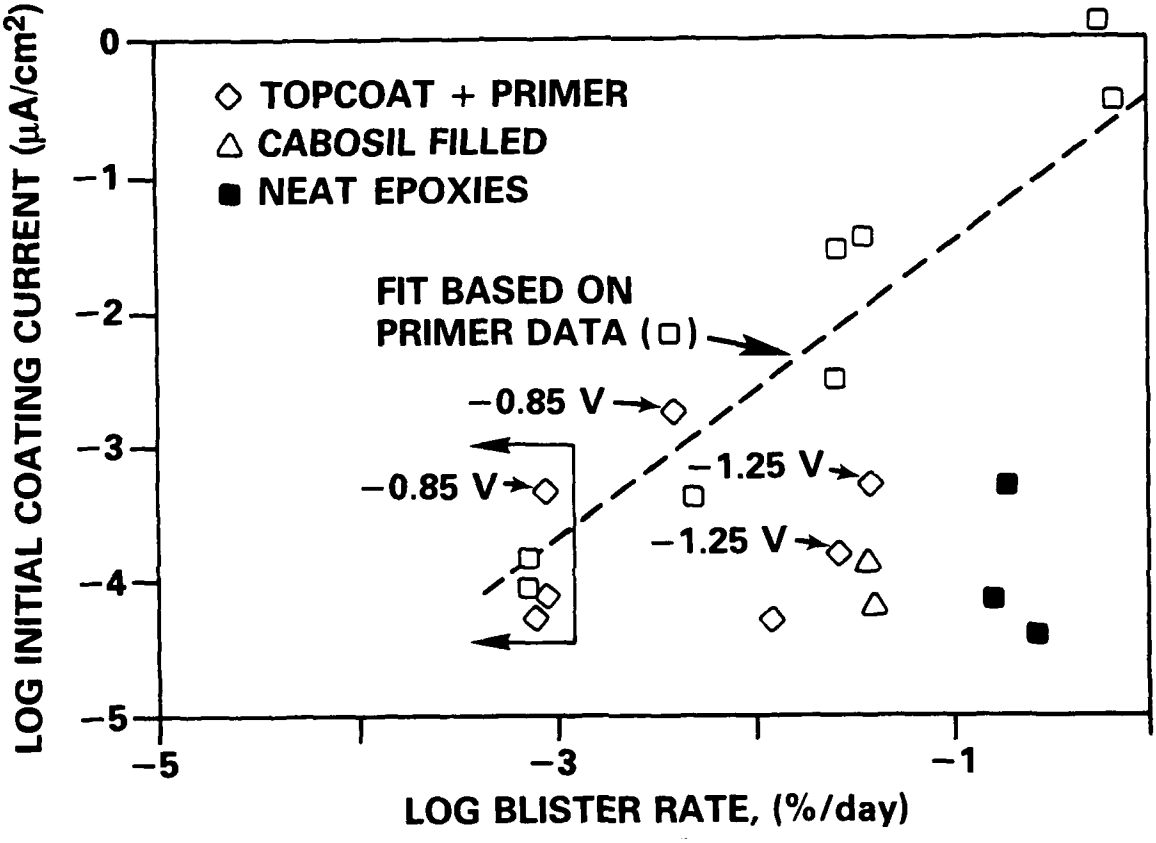

Fig. 8. K/init. R_{MAX} and blister area growth.

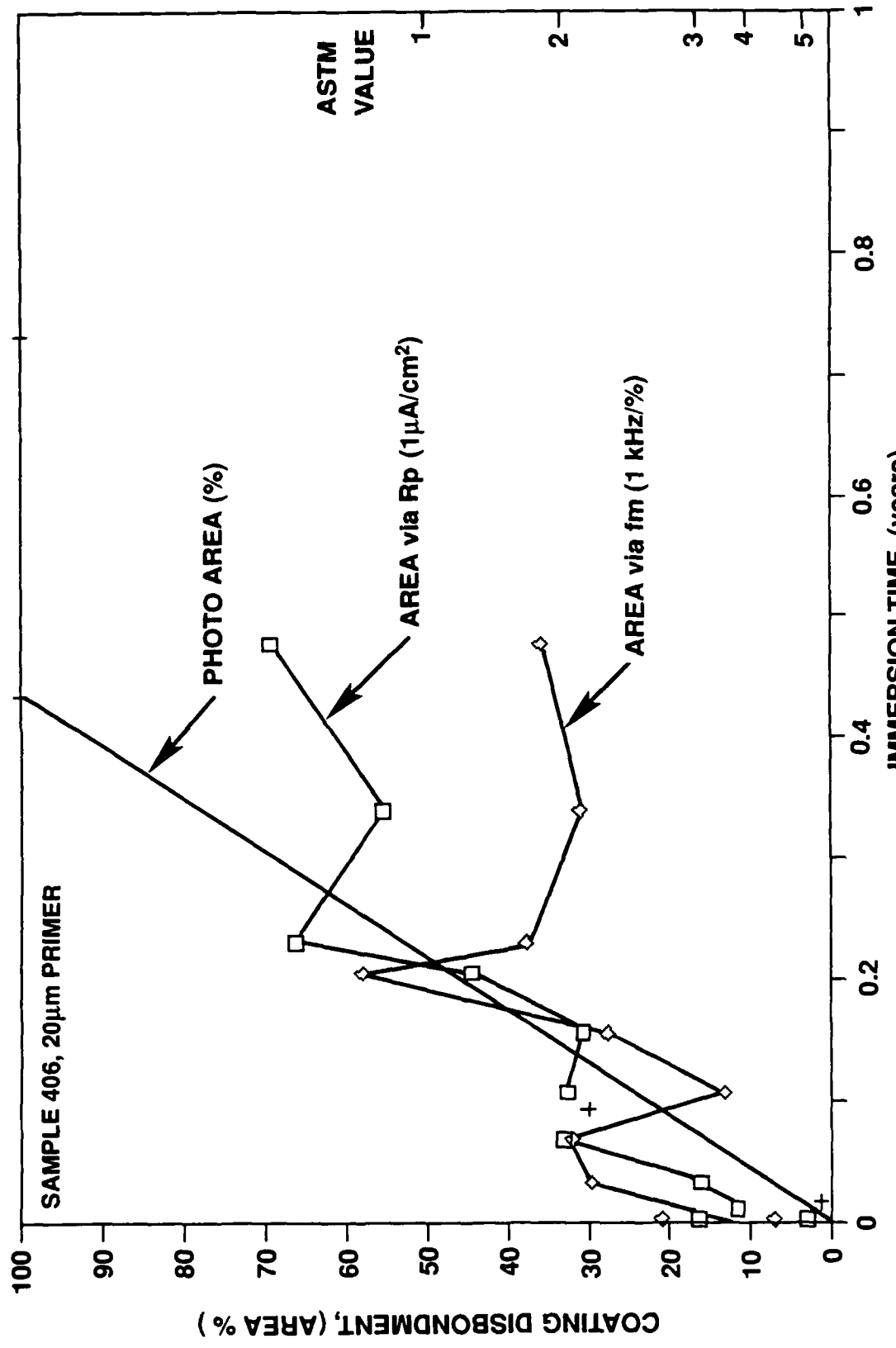

Fig. 9. Comparison of disbonded area-time values by EIS and visual techniques.

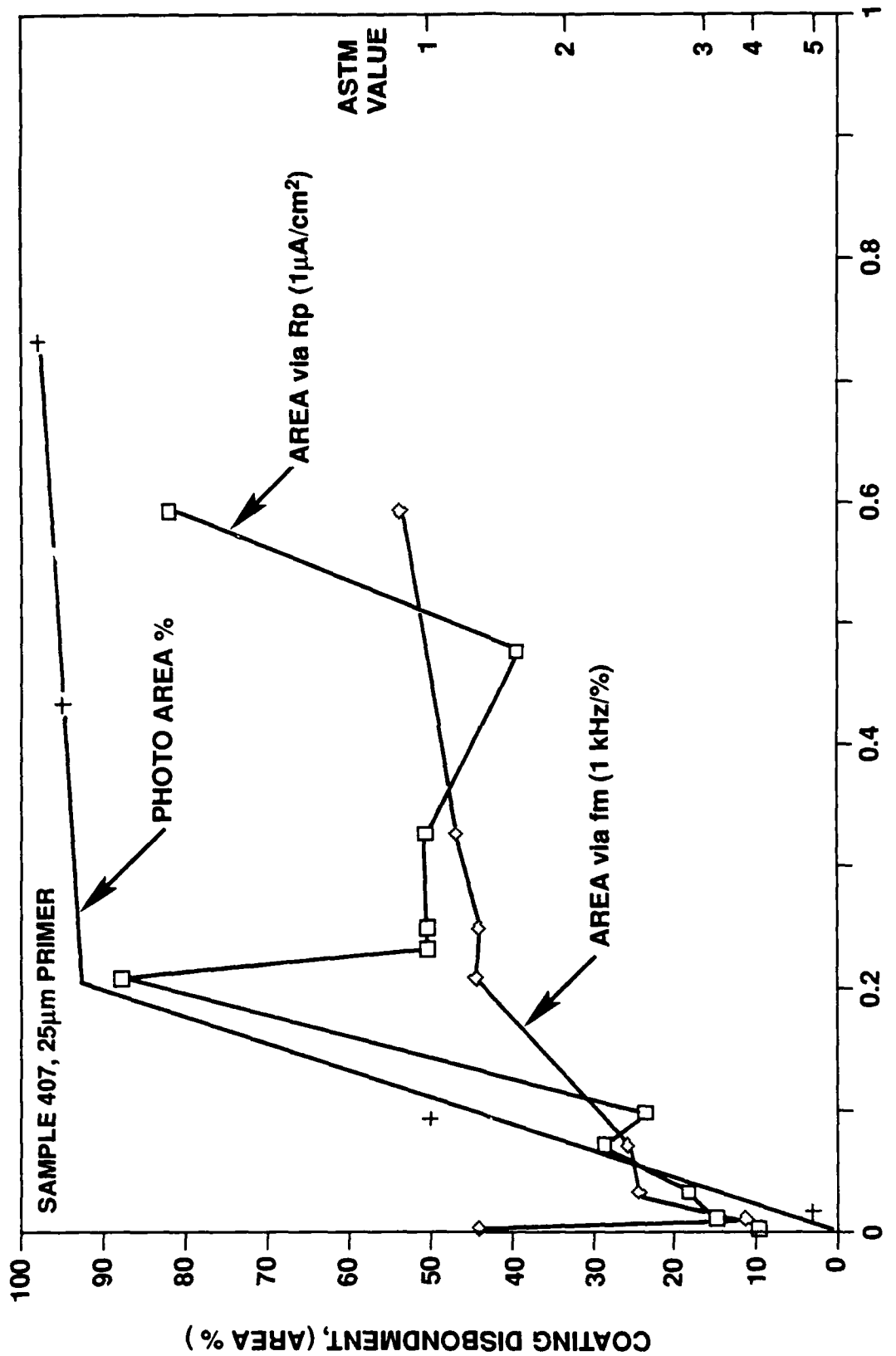

Fig. 10. Comparison of disbonded area-time values by EIS and visual techniques.

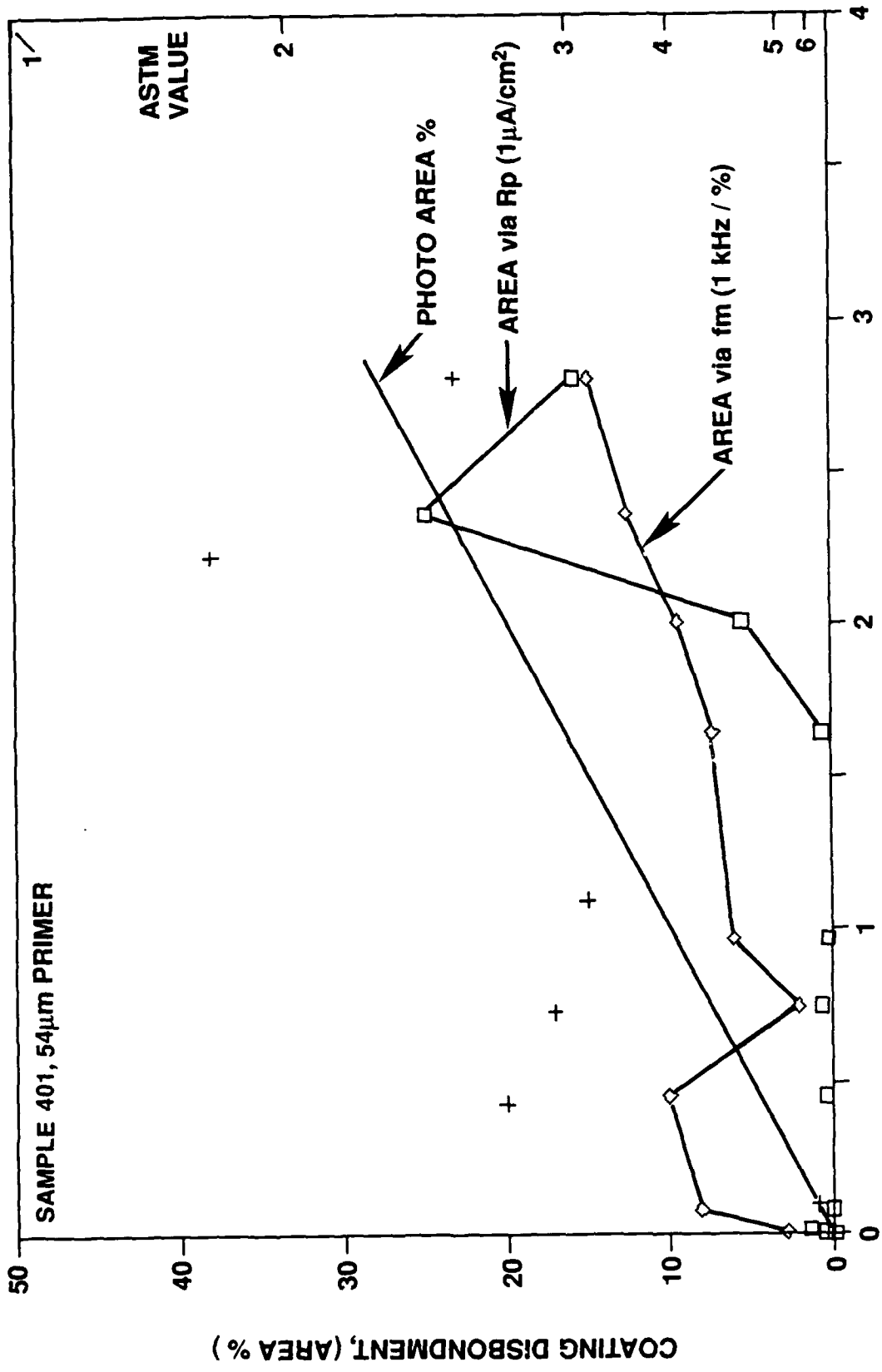

Fig. 11. Comparison of disbonded area-time values by EIS and visual techniques.

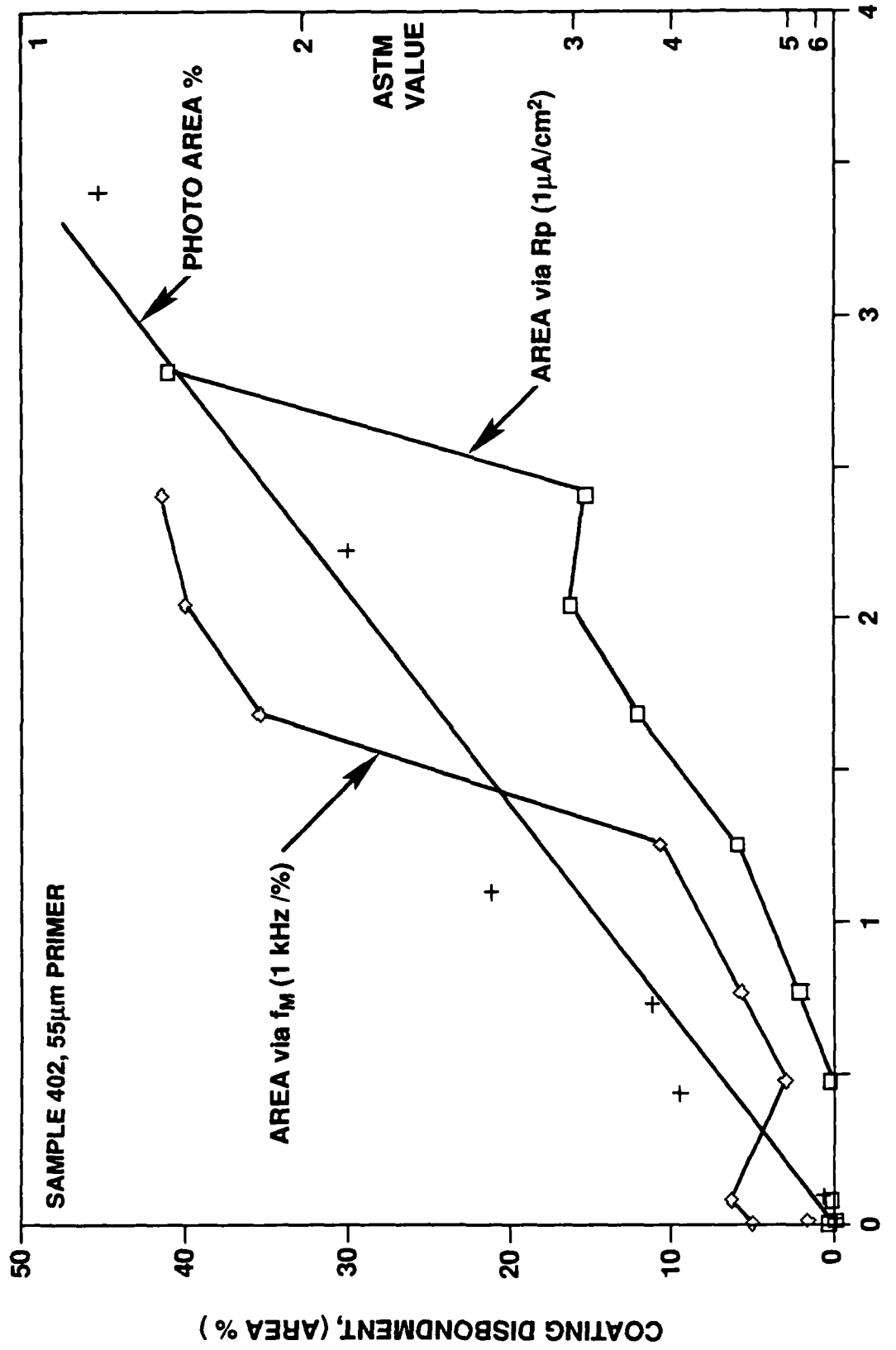

Fig. 12 Comparison of disbonded area-time values by EIS and visual techniques.

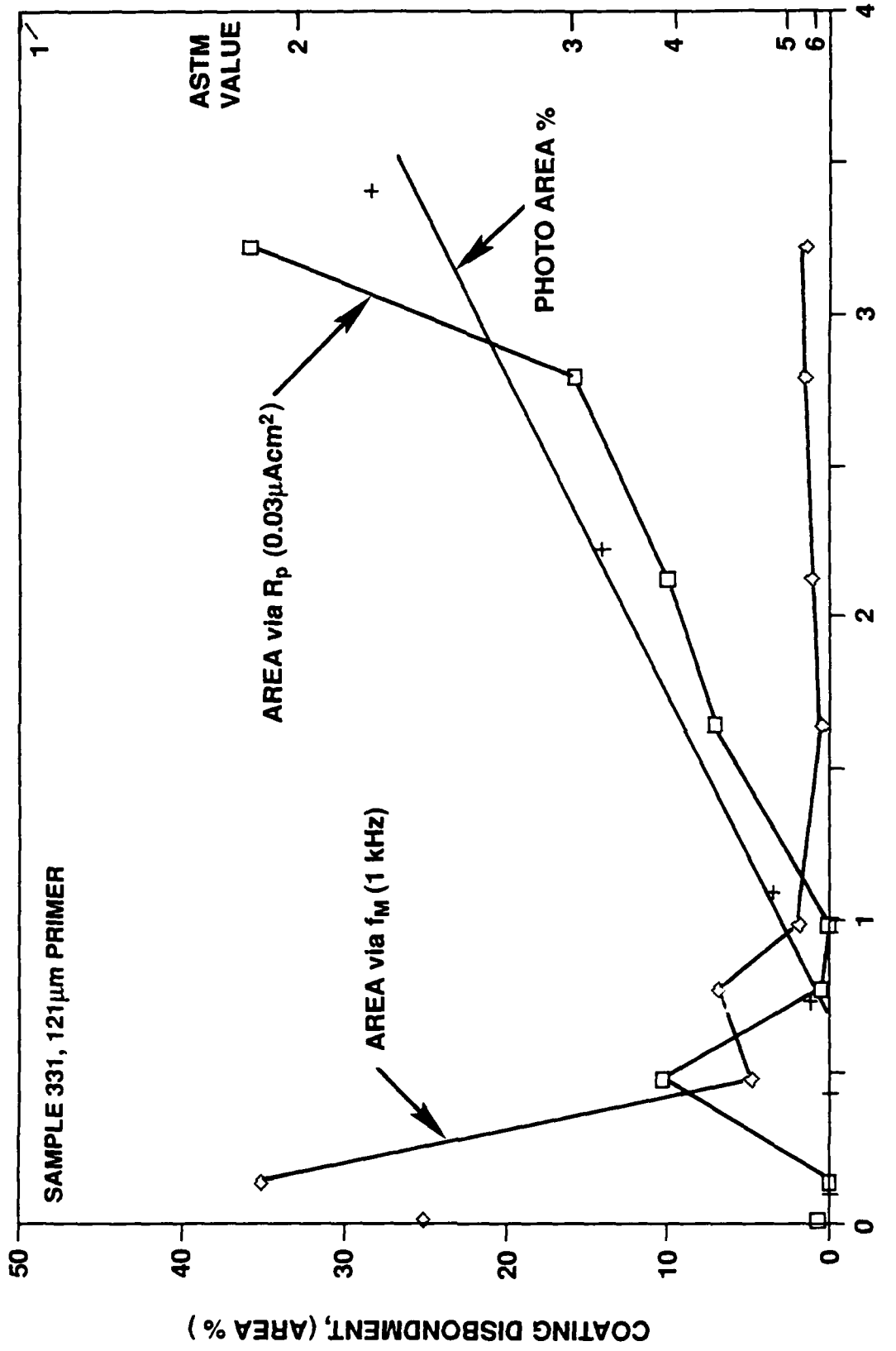

Fig. 13. Comparison of disbonded area-time values by EIS and visual techniques.

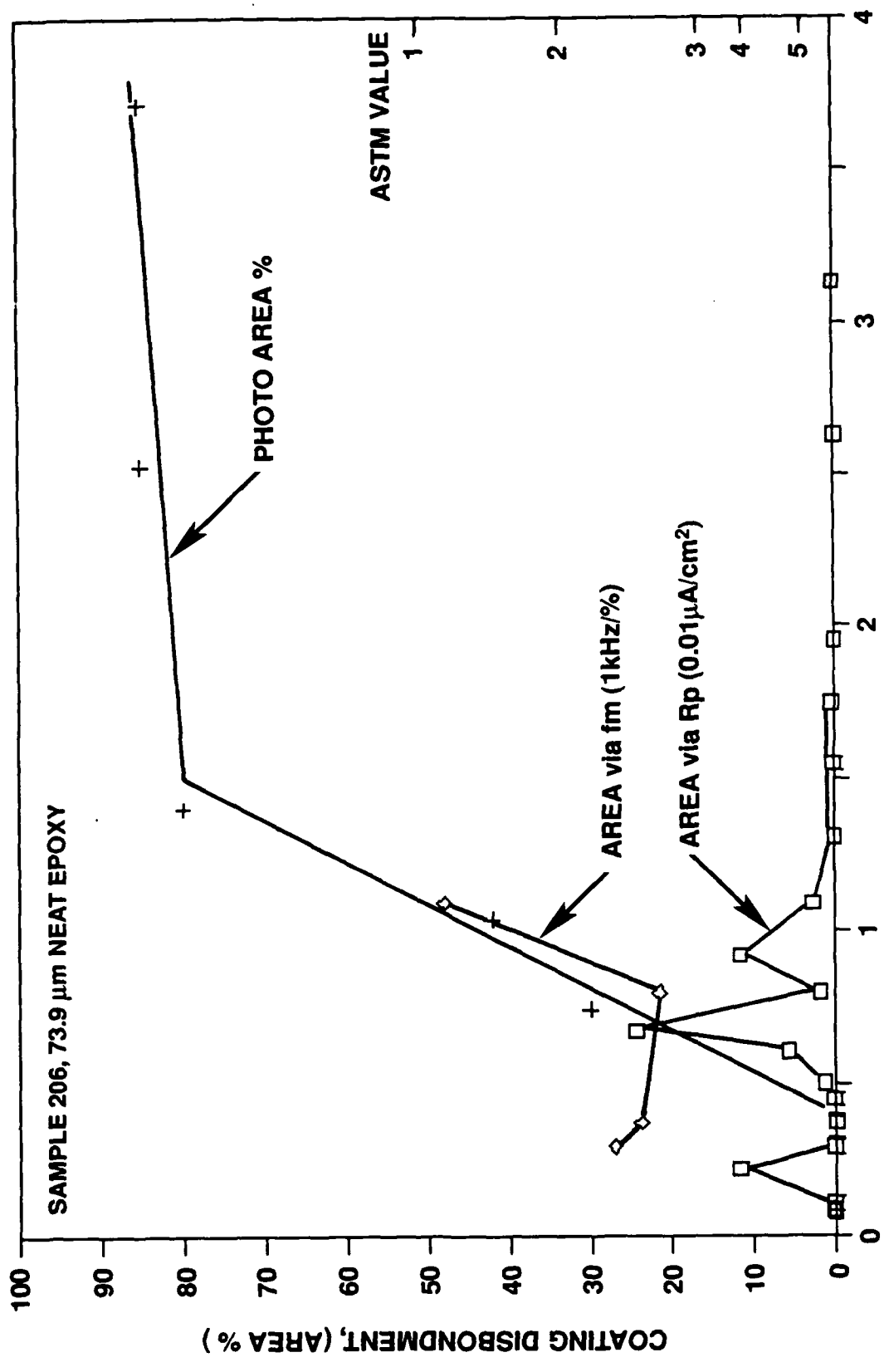

Fig. 14. Comparison of disbonded area-time values by EIS and visual techniques.

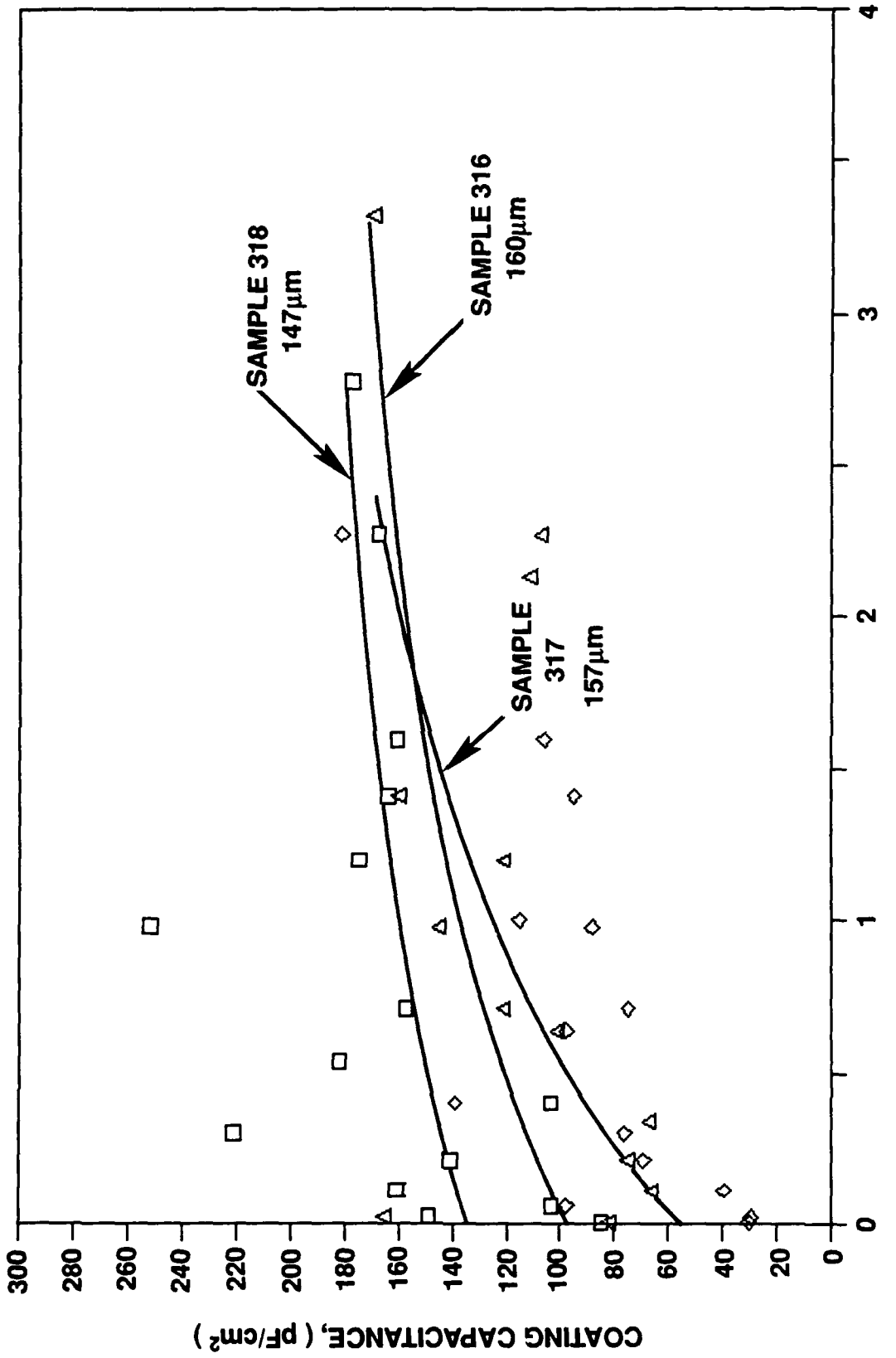

Fig. 15. Primer plus topcoat samples; coating capacitance-time data.

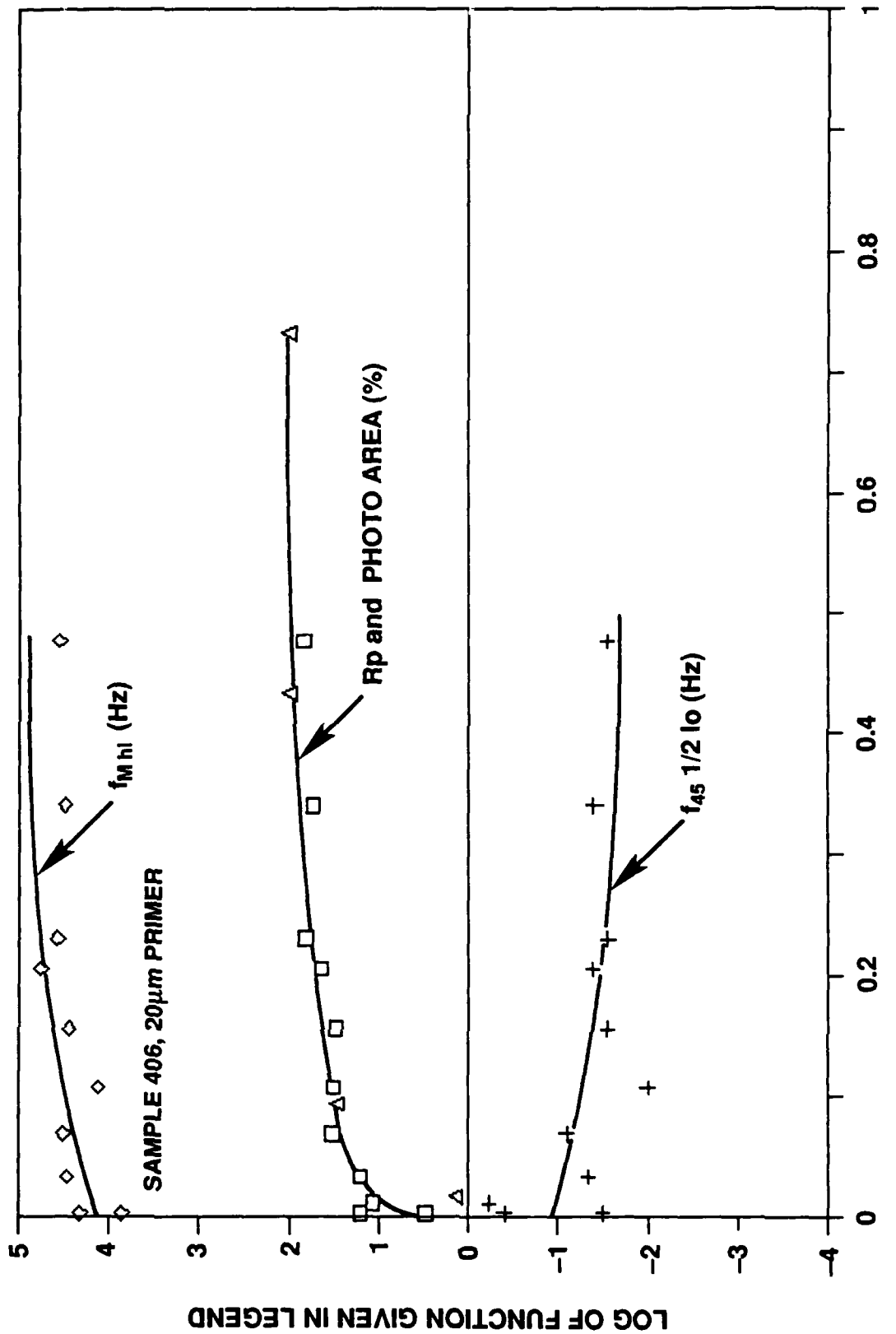

Fig. 16. Comparison of disbonded area and EIS parameters.

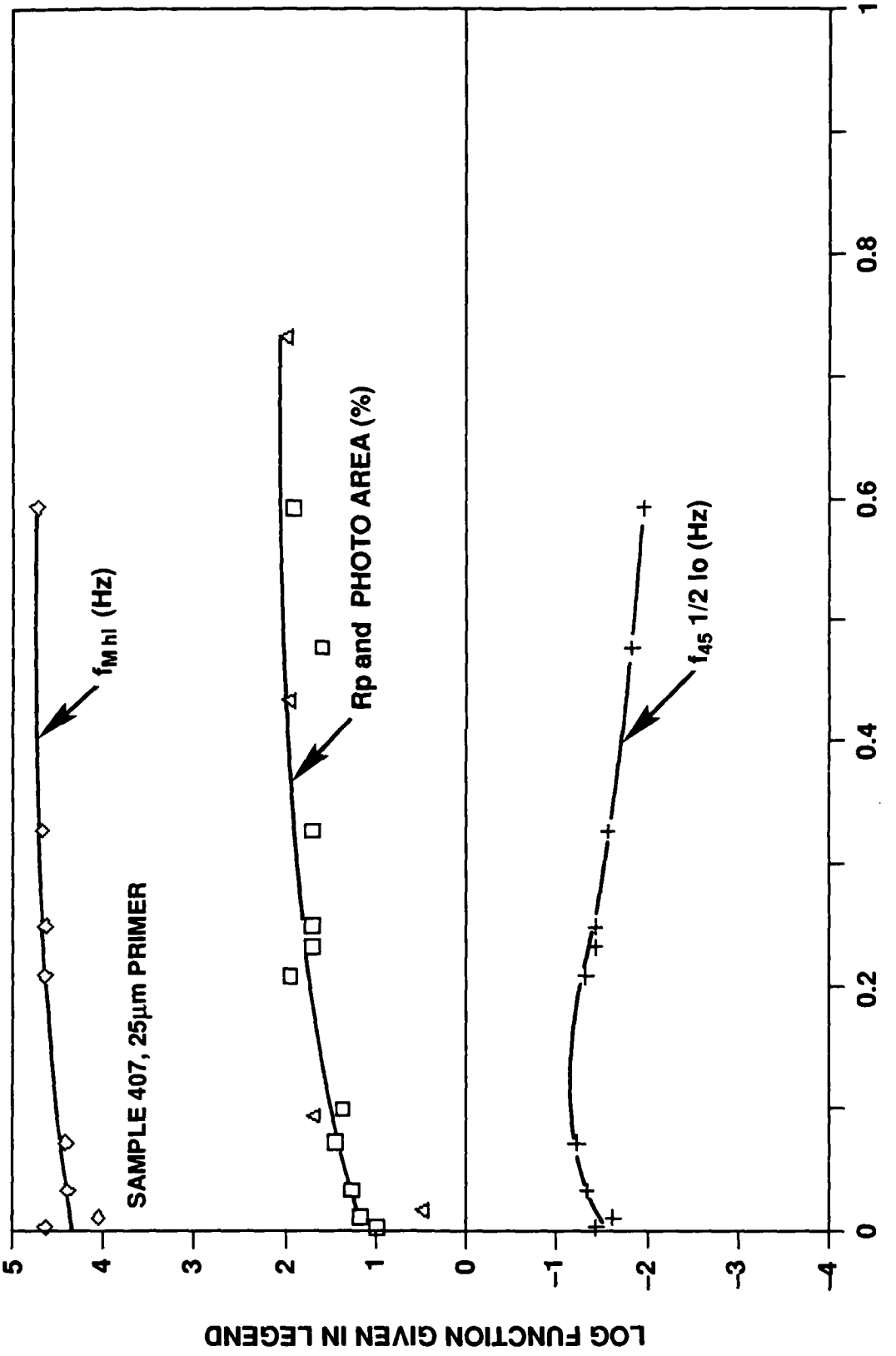

Fig. 17. Comparison of disbonded area and EIS parameters.

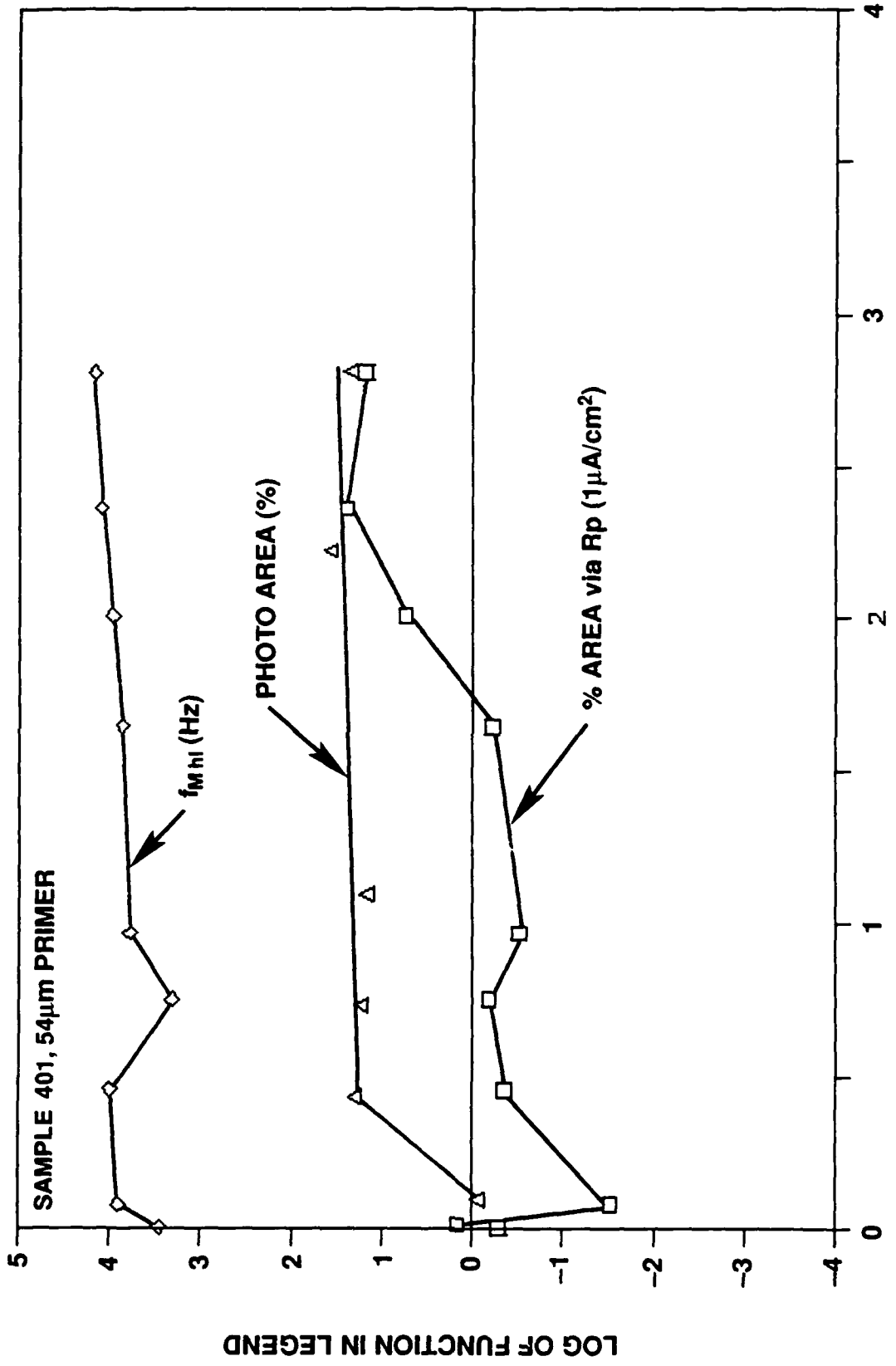

Fig. 18. Comparison of disbonded area and EIS parameters.

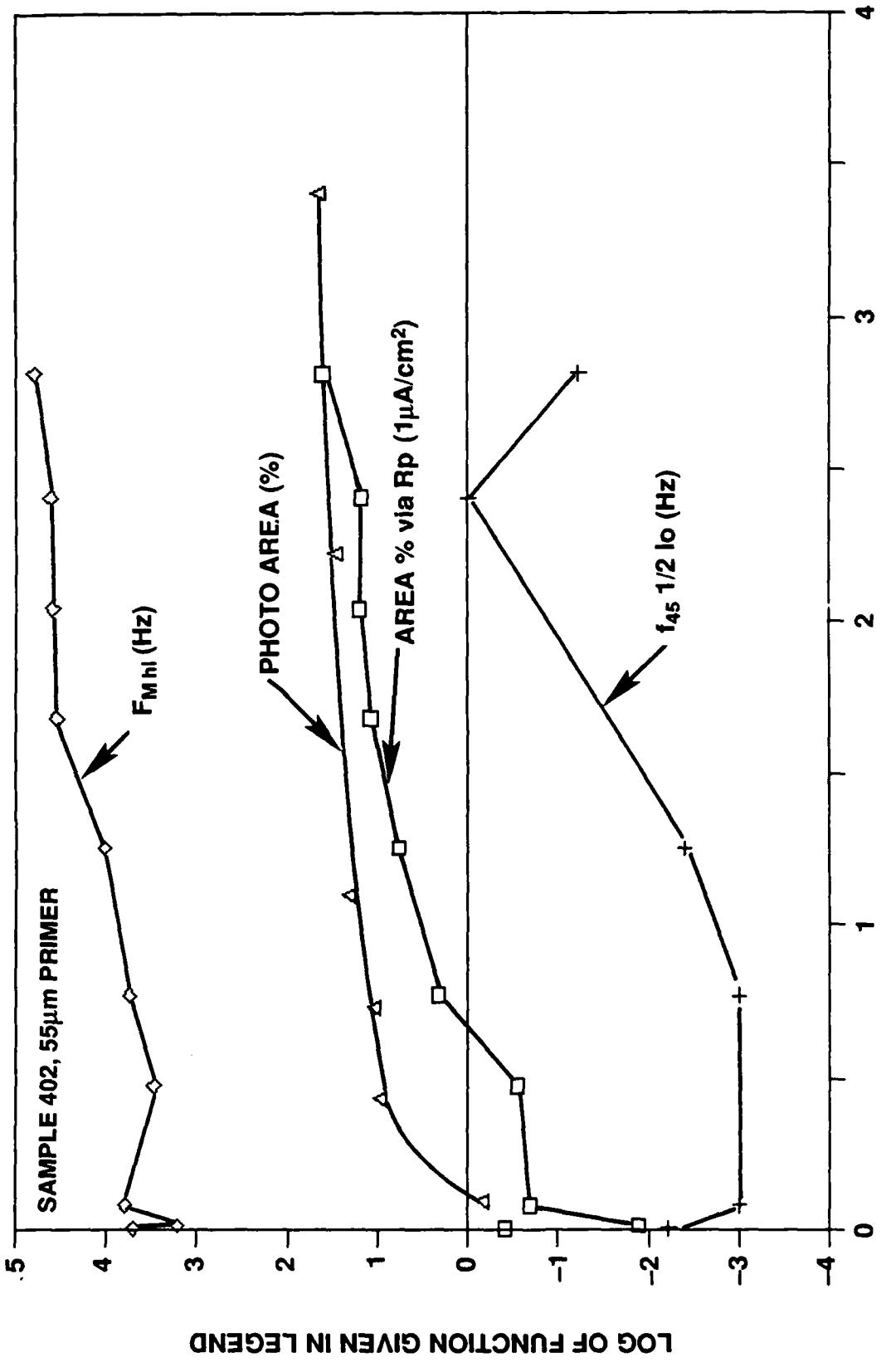

Fig. 19. Comparison of disbonded area and EIS parameters.

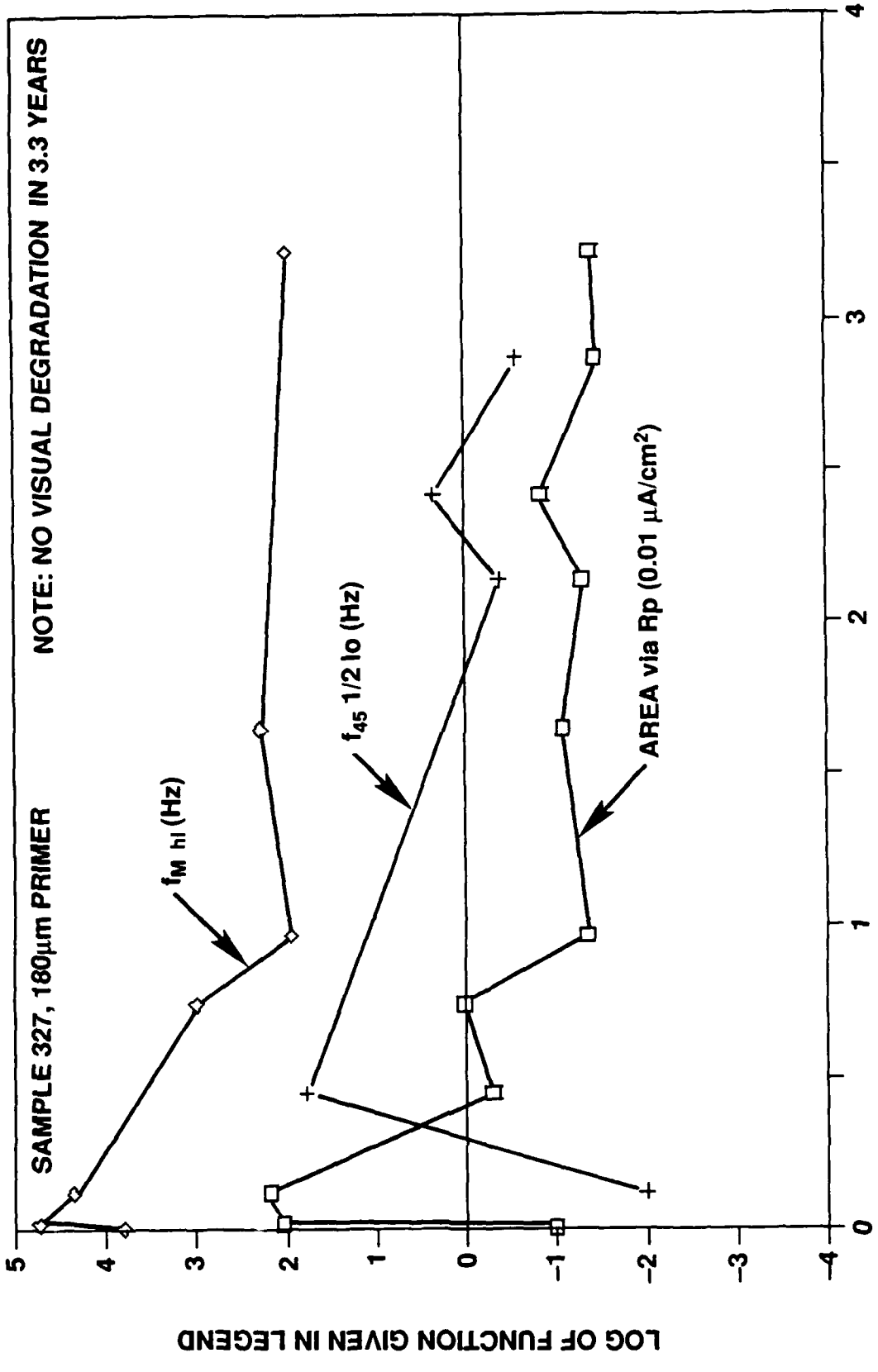

Fig. 20. Comparison of disbonded area and EIS parameters.

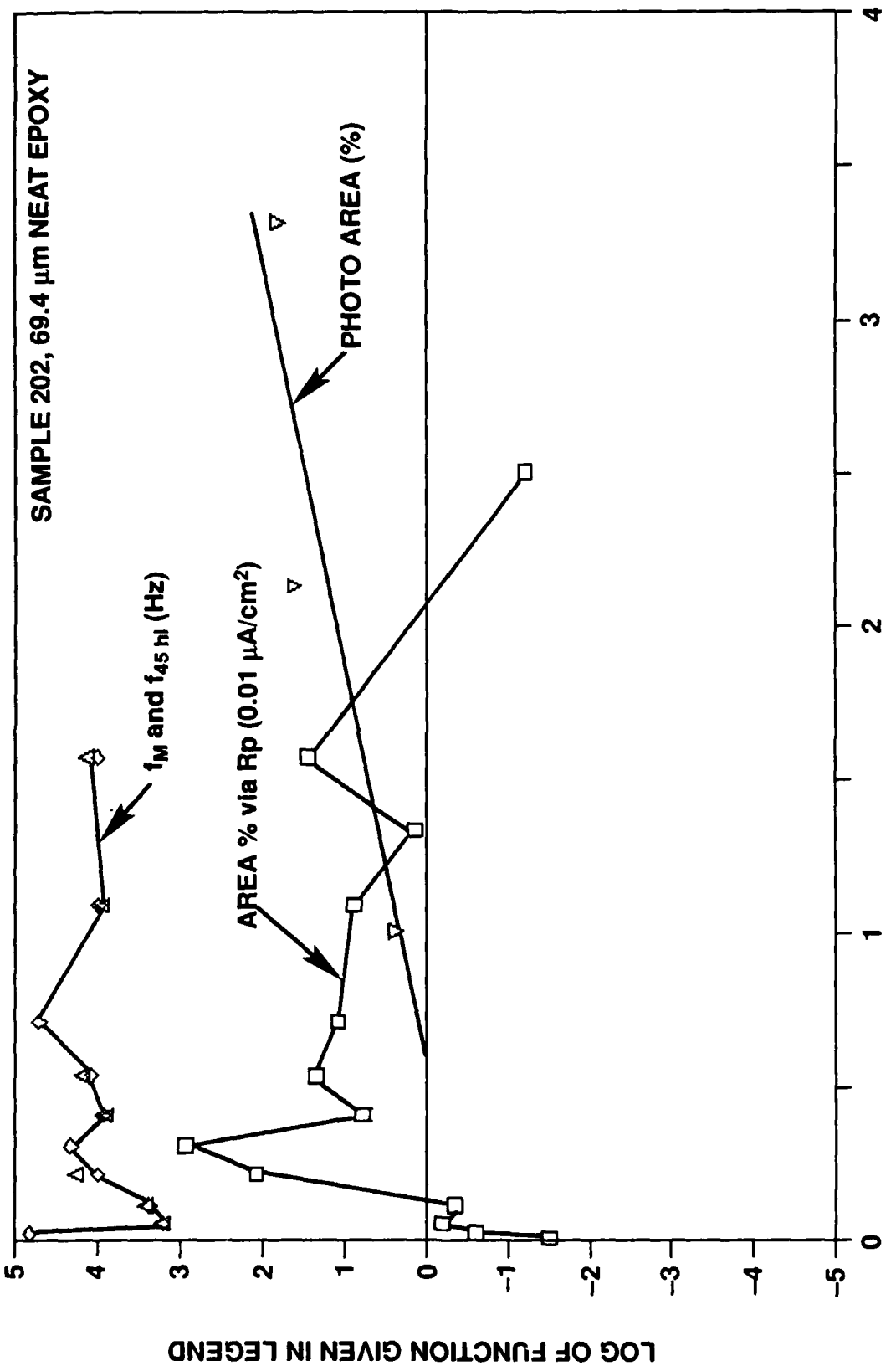

Fig. 21. Comparison of disbonded area and EIS parameters.

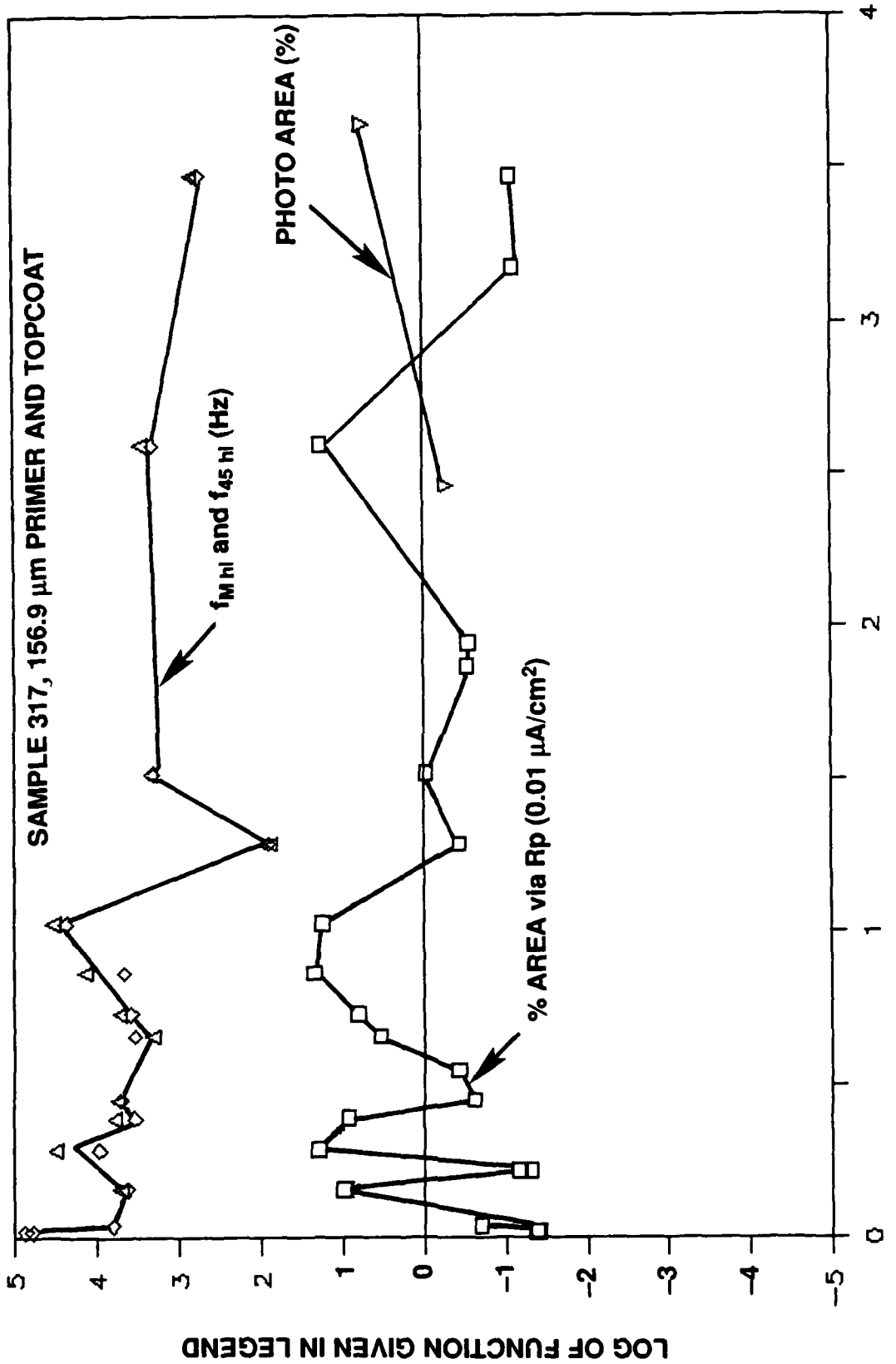

Fig. 22. Comparison of disbonded area and EIS parameters.

REFERENCES

1. Scully, J.R., DTNSRDC/SME-85/01, David W. Taylor Naval Ship Research and Development Center, Annapolis, MD 21402 (Aug 1985).
2. Scully, J.R., DTNSRDC/SME-86/006, David W. Taylor Naval Ship Research and Development Center, Annapolis, MD 21402 (Sept 1986).
3. Scully, J.R., DTRC/SME-86/108, David Taylor Research Center, Annapolis, MD 21402 (Apr 1988).
4. Hack, H.P. and J.R. Scully, submitted for review to Corrosion-NACE (June 1989).
5. Mansfeld, F., M.W. Kendig, and S. Tsai, Corrosion-NACE, 38, No. 9, pp. 478-485, (Sept 1982).
6. Callow, L.M. and J.D. Scantlebury, J. Oil & Col. Chem. Assn. *64* (Part 1, pp. 83-86), (Part 2, pp. 119-123) (Part 3, pp. 140-143) (1981).
7. McIntyre, J.F. and H. Leidheiser, Jr., J. Electrochem. Soc., 133, No. 1, pp. 43-48 (Jan 1986).
8. Haruyama, S., M. Asari, and T. Tsuru, pp. 197-207, in Proc. Vol. 87-2, "Corr. Prot. by Org. Coats," M. Kendig and H. Leidheiser, eds., ECS (1987).
9. Walter, G.W., Corr. Sci., 26, No. 9, pp. 681-703 (1986).
10. Sluyters, J.H. and J.J.C. Oomen, Recueil, 79, Nos. 9/10, pp. 1101-1110 (1960).
11. Grahame, D.C., Chem. Rev., 41, pp. 441-501 (1947).
12. Murray, J.N., P.J. Moran, and E. Gileadi, Corrosion, 44, No. 8, pp. 533-538 (Aug 1988).
13. Leidheiser, H. Jr., pp. 143-170 in "Corrosion Control by Coatings," H. Leidheiser, Jr., ed., Science Press, Princeton, NJ (1979).
14. Bacon, R.C., J.J. Smith and F.M. Rugg, Ind. Eng. Chem. 40, No. 1, pp. 161-167 (Jan 1948).
15. Murray, J.N. and P.J. Moran, accepted for publication in Corrosion-NACE (1989).
16. Scully, J.R., Paper 222, Corrosion 86, NACE (Mar 1986).
17. Scully, J.R., JECS, 136, No. 4, pp. 979-990 (Apr 1989).
18. Parks, J. and H. Leidheiser, Jr.; Ind. Eng. Prod. Res. Dev., 25, No. 1, pp. 1-6 (1986).
19. Thornton, J.S., R.E. Montgomery, and J.F. Cartier, NRL Memorandum Report 5584, Naval Research Laboratory, Washington, DC (30 May 1985).
20. Mayne, J.E.O. and D.J. Mills, J. Oil and Col. Chem. Assn., 58, No. 5, pp. 155-159, (1975).
21. Handbook of Chem. and Phys., p. E-35, 45th edition., CRP (1964).
22. Meredith, R.E. and C.W. Tobias, JECS, 110, No. 12, pp. 1257-1260 (Dec 1963).

INITIAL DISTRIBUTION

Copies

1 DARPA
1400 Wilson Blvd.
Arlington, VA 22209
Attn: Dr. P. Parrish

2 Office of Naval Research
800 N. Quincy Street
Arlington, VA 22217
Attn: Dr. Sedriks (Code 1131)
Dr. S. Fishman (Code 1131)

1 NRL
Dr. E. McCafferty, Code 6310

2 Commander
Naval Surface Weapons Center
Silver Spring, MD 20903
Attn: Dr. Vasanth (Code R33)
Dr. Tydings (Code R32)

1 Commander
Naval Surface Weapons Center
Dahlgren, VA 22448
Attn: Dr. Bettadapur (Code C53)

3 Commander
Naval Civil Engineering Lab
Port Hueneme, CA 93043
Attn: Dr. R. Drisko,
Mr. D. Zarate,
Mr. J. Jenkins

1 Commander
Naval Air Development Center
Warminster, PA 18974
Attn: Dr. Agarwala

1 Commander
Naval Ocean Systems Center
San Diego, CA 92152
Attn:. Mr. Chase (Code 932)

2 Department of the Army
AMTL
SLCMT-MCM-SB
Watertown, MA 02172
Attn: Mr. M. Levy
Dr. E. Wright

2 U.S. Army Research Office
Associate Director of Metallurgy
and Materials
Science Division
P.O. Box 1221
Triangle Park, NC 27709
Attn: Dr. John Hurt
Dr. Robert Rebar

12 Defense Technical Info Center
Cameron Station
Alexandria, VA 22314

3 Commanding Officer
Air Force Materials Laboratory
Wright-Patterson AFB
Dayton, OH 45433
Attn: Mr. Meyer (Code MLSA)

1 Air Force Office of
Scientific Research
Bolling Air Force Base
Washington, D.C. 20332
Attn: Dr. A. Rosenstein

3 National Insititute of Standards and Technology
Gaithersburg, MD 20899
Attn: Dr. N.E. Pugh
Dr. U. Bertocci
Dr. J.W. Martin

1 Monsanto Company
800 N. Lindbergh Blvd.
St. Louis, MO 63167
Attn: Dr. David Silverman

1 Electrical Technology Corp.
1601 Dexter Avenue
N. Seattle, WA 98109
Attn: Dr. Theodore Beck

1 Center for Surface and Coating Research
Sinclair Laboratory 7
Lehigh University
Bethlehem, PA 18015
Attn: Dr. Richard Granata
Dr. H. Leidheiser

2 EG&G Princeton Applied Research
P.O. Box 25651
Princeton, N.J. 08540
Attn: Mr. Marc Rothstein
Mr. Bill Eggers

1 Martin Marietta Laboratories
1450 South Rolling Road
Baltimore, MD 21227-3898
Attn: Dr. W. Moshier

1 University of Nevada
Reno, NV 89557
Attn: Dr. Denny Jones

1 Steel Structures Painting Council
4400 Fifth Avenue
Pittsburgh, PA 15213
Attn: Dr. Bernard Appleman

2 The Johns Hopkins University
Corrosion & Electrochemistry Research Center
Charles and 34th Streets
Baltimore, MD 21218
Attn: Dr. J. Kruger

1 Rohm and Haas Company
Research Division
727 Norristown Road
Spring House, PA 19477
Attn: Dr. Bart S. Frechem

1 Sandia National Laboratory
Org. No. 1832
P.O. Bos 5800
Albuquerque, NM 87185
Attn: Dr. John Scully

CENTER DISTRIBUTION

Copies	Code	Name
1	015	Moran
1	0115	Caplan
1	28	Wacker
1	2801	Crisci
1	2801	Ventriglio
1	2801	Moran
1	2802	Morton
1	2803	Cavallaro
1	2809	Malec
5	281	Czyryca
5	2813	Ferrara
10	2813	Hack

1	2814	Montemarano
1	283	Singerman
1	284	Fischer
5	2841	Montemarano Ross Laster Loeb Mihm
1	342.2	TIC
2	3431	Office Services